

## Reporting Summary

Nature Portfolio wishes to improve the reproducibility of the work that we publish. This form provides structure for consistency and transparency in reporting. For further information on Nature Portfolio policies, see our [Editorial Policies](#) and the [Editorial Policy Checklist](#).

### Statistics

For all statistical analyses, confirm that the following items are present in the figure legend, table legend, main text, or Methods section.

n/a Confirmed

- |                                     |                                     |  |
|-------------------------------------|-------------------------------------|--|
| <input type="checkbox"/>            | <input checked="" type="checkbox"/> | The exact sample size ( $n$ ) for each experimental group/condition, given as a discrete number and unit of measurement  |
| <input type="checkbox"/>            | <input checked="" type="checkbox"/> | A statement on whether measurements were taken from distinct samples or whether the same sample was measured repeatedly  |
| <input type="checkbox"/>            | <input checked="" type="checkbox"/> | The statistical test(s) used AND whether they are one- or two-sided<br><i>Only common tests should be described solely by name; describe more complex techniques in the Methods section.</i>   |
| <input checked="" type="checkbox"/> | <input type="checkbox"/>            | A description of all covariates tested   |
| <input type="checkbox"/>            | <input checked="" type="checkbox"/> | A description of any assumptions or corrections, such as tests of normality and adjustment for multiple comparisons  |
| <input type="checkbox"/>            | <input checked="" type="checkbox"/> | A full description of the statistical parameters including central tendency (e.g. means) or other basic estimates (e.g. regression coefficient) AND variation (e.g. standard deviation) or associated estimates of uncertainty (e.g. confidence intervals) |
| <input type="checkbox"/>            | <input checked="" type="checkbox"/> | For null hypothesis testing, the test statistic (e.g. $F$ , $t$ , $r$ ) with confidence intervals, effect sizes, degrees of freedom and $P$ value noted<br><i>Give <math>P</math> values as exact values whenever suitable.</i>                            |
| <input checked="" type="checkbox"/> | <input type="checkbox"/>            | For Bayesian analysis, information on the choice of priors and Markov chain Monte Carlo settings   |
| <input type="checkbox"/>            | <input checked="" type="checkbox"/> | For hierarchical and complex designs, identification of the appropriate level for tests and full reporting of outcomes   |
| <input type="checkbox"/>            | <input checked="" type="checkbox"/> | Estimates of effect sizes (e.g. Cohen's $d$ , Pearson's $r$ ), indicating how they were calculated   |

Our web collection on [statistics for biologists](#) contains articles on many of the points above.

### Software and code

Policy information about [availability of computer code](#)

|                 |   |
|-----------------|---|
| Data collection | For MS acquisition, the XcaliburTM 4.3 software of Thermo Fisher mass spectrometers was used.<br>Cryo-EM data collection was performed using software EPU (v2.3, Thermo Fisher) and CETCORPLUS 4.6.9 (CEOS).<br>Stopped flow data was collected using Pro-Data SX2.5.1852.0 (Applied Photophysics).<br>Fluorescent peptides were detected using Starion IR/FLA-9000 scanner (FujiFilm).<br>Microscopy images were acquired using Zen Black 2.3 (Zeiss).   |
| Data analysis   | No new code was generated in this study.<br>MS data were processed using MaxQuant (v2.0.1.0 and 2.1.4.0), Spectronaut (v17.1.22), PEAKS (PROSIT integrated, v10.5), Perseus (v1.6.15.0) and Skyline (v24.1.0.199).<br>Missense peptides were identified using a published Python script (Mordret et al., 2019).<br>Cryo-EM data were processed using Automatch 0.56, RELION (v3.1 and 5.0), MotionCor2, CTFFIND v4.1 and ChimeraX (v1.8.1.10.1).<br>Atomic models were refined using PHENIX (v 1.20.1) and WinCoot (v0.9.8.95).<br>Microscopy image analysis was performed using Fiji (v2.14) and MicrobeJ (v5.14p).<br>SDS PAGES were densitometrically analyzed using Multi Gauge software (FujiFilm).<br>Kinetic time courses were exponentially fitted using GraphPad Prism. In general, data were visualized in GraphPad Prism (v 10.2.3), Biorender and CorelDRAW (v 26.1.0.143).<br>All software tools are publicly available. |

For manuscripts utilizing custom algorithms or software that are central to the research but not yet described in published literature, software must be made available to editors and reviewers. We strongly encourage code deposition in a community repository (e.g. GitHub). See the Nature Portfolio [guidelines for submitting code & software](#) for further information.

## Data

Policy information about [availability of data](#)

All manuscripts must include a [data availability statement](#). This statement should provide the following information, where applicable:

- Accession codes, unique identifiers, or web links for publicly available datasets
- A description of any restrictions on data availability
- For clinical datasets or third party data, please ensure that the statement adheres to our [policy](#)

All data supporting the findings of this study are available within the article, its Supplementary Information, or in the indicated public repositories. The corresponding authors are available for clarification regarding data content or access. Source data are provided with this paper. No new code was generated in this study. The targeted MS data generated in this study have been deposited to the ProteomeXchange consortium via the Panorama partner repository under the accession code PXD063129. All proteomics data generated in this study have been deposited to the ProteomeXchange consortium via the PRIDE partner repository under the accession codes PXD061583 and PXD067947. Raw microscopy images have been deposited to Zenodo under the doi 10.5281/zenodo.17087887. The cryo-EM maps/associated coordinates of atomic models generated in this study have been deposited in the Electron Microscopy Data Bank/Protein Data Bank under the following accession codes: EMDB: 55123; EMDB: 55124; EMDB 55125; PDB: 9RTU; EMDB: 54253 and PDB: 9RTV; EMDB: 54254. Previously published atomic coordinates from the Protein Data Bank (PDB accession codes 7PJS, 8CGJ, 8CEP, 8CA7, 8CF1, 7PJV and 7PJW) were used for illustrations and initial atomic model fitting. Plasmids and bacterial strains generated in this study are available from the corresponding authors upon reasonable request.

## Research involving human participants, their data, or biological material

Policy information about studies with [human participants or human data](#). See also policy information about [sex, gender \(identity/presentation\), and sexual orientation](#) and [race, ethnicity and racism](#).

|  |    |
|--|----|
| Reporting on sex and gender  | NA |
| Reporting on race, ethnicity, or other socially relevant groupings | NA |
| Population characteristics   | NA |
| Recruitment  | NA |
| Ethics oversight   | NA |

Note that full information on the approval of the study protocol must also be provided in the manuscript.

## Field-specific reporting

Please select the one below that is the best fit for your research. If you are not sure, read the appropriate sections before making your selection.

☒ Life sciences ☐ Behavioural & social sciences ☐ Ecological, evolutionary & environmental sciences

For a reference copy of the document with all sections, see [nature.com/documents/nr-reporting-summary-flat.pdf](https://www.nature.com/documents/nr-reporting-summary-flat.pdf)

## Life sciences study design

All studies must disclose on these points even when the disclosure is negative.

|                 |  |
|-----------------|--|
| Sample size     | Due to the mechanistic and exploratory nature of our analysis, no statistical methods were used to predetermine sample sizes. Effect sizes and variance estimates were unknown for key measurements (e.g., missense error suppression). We followed established microbiology and proteomics practices to ensure reproducibility and statistical robustness. All results were confirmed across biological replicates and substantiated using orthogonal methods.  |
| Data exclusions | No data was excluded from analysis.  |
| Replication     | The core findings (e.g. EF-G resistance variants can silence corrupted ribosomes and shield the cell against aminoglycosides) are supported by orthogonal approaches including quantitative MS, live-cell imaging, in-vitro translation and translation kinetics, and cryo-EM. All experiments were replicated at least three times with similar results (n as indicated in the figure captions). Biological replicates include individual cell growth, drug treatment, sample processing and data acquisition. Technical replicates are based on repeatedly analyzed samples. All replication attempts were successful. |
| Randomization   | Experiments were not randomized, due to the mechanistic nature of the study and because sample identity is inferable from data structure.  |
| Blinding        | Investigators were not blinded, due to the mechanistic nature of the study and because sample identity is inferable from data structure.   |

# Behavioural & social sciences study design

All studies must disclose on these points even when the disclosure is negative.

|                   |   |
|-------------------|---|
| Study description | Briefly describe the study type including whether data are quantitative, qualitative, or mixed-methods (e.g. qualitative cross-sectional, quantitative experimental, mixed-methods case study).   |
| Research sample   | State the research sample (e.g. Harvard university undergraduates, villagers in rural India) and provide relevant demographic information (e.g. age, sex) and indicate whether the sample is representative. Provide a rationale for the study sample chosen. For studies involving existing datasets, please describe the dataset and source.  |
| Sampling strategy | Describe the sampling procedure (e.g. random, snowball, stratified, convenience). Describe the statistical methods that were used to predetermine sample size OR if no sample-size calculation was performed, describe how sample sizes were chosen and provide a rationale for why these sample sizes are sufficient. For qualitative data, please indicate whether data saturation was considered, and what criteria were used to decide that no further sampling was needed. |
| Data collection   | Provide details about the data collection procedure, including the instruments or devices used to record the data (e.g. pen and paper, computer, eye tracker, video or audio equipment) whether anyone was present besides the participant(s) and the researcher, and whether the researcher was blind to experimental condition and/or the study hypothesis during data collection.  |
| Timing            | Indicate the start and stop dates of data collection. If there is a gap between collection periods, state the dates for each sample cohort.   |
| Data exclusions   | If no data were excluded from the analyses, state so OR if data were excluded, provide the exact number of exclusions and the rationale behind them, indicating whether exclusion criteria were pre-established.  |
| Non-participation | State how many participants dropped out/declined participation and the reason(s) given OR provide response rate OR state that no participants dropped out/declined participation.   |
| Randomization     | If participants were not allocated into experimental groups, state so OR describe how participants were allocated to groups, and if allocation was not random, describe how covariates were controlled.   |

# Ecological, evolutionary & environmental sciences study design

All studies must disclose on these points even when the disclosure is negative.

|                          |   |
|--------------------------|---|
| Study description        | Briefly describe the study. For quantitative data include treatment factors and interactions, design structure (e.g. factorial, nested, hierarchical), nature and number of experimental units and replicates.  |
| Research sample          | Describe the research sample (e.g. a group of tagged <i>Passer domesticus</i> , all <i>Stenocereus thurberi</i> within Organ Pipe Cactus National Monument), and provide a rationale for the sample choice. When relevant, describe the organism taxa, source, sex, age range and any manipulations. State what population the sample is meant to represent when applicable. For studies involving existing datasets, describe the data and its source. |
| Sampling strategy        | Note the sampling procedure. Describe the statistical methods that were used to predetermine sample size OR if no sample-size calculation was performed, describe how sample sizes were chosen and provide a rationale for why these sample sizes are sufficient.   |
| Data collection          | Describe the data collection procedure, including who recorded the data and how.  |
| Timing and spatial scale | Indicate the start and stop dates of data collection, noting the frequency and periodicity of sampling and providing a rationale for these choices. If there is a gap between collection periods, state the dates for each sample cohort. Specify the spatial scale from which the data are taken   |
| Data exclusions          | If no data were excluded from the analyses, state so OR if data were excluded, describe the exclusions and the rationale behind them, indicating whether exclusion criteria were pre-established.   |
| Reproducibility          | Describe the measures taken to verify the reproducibility of experimental findings. For each experiment, note whether any attempts to repeat the experiment failed OR state that all attempts to repeat the experiment were successful.   |
| Randomization            | Describe how samples/organisms/participants were allocated into groups. If allocation was not random, describe how covariates were controlled. If this is not relevant to your study, explain why.  |
| Blinding                 | Describe the extent of blinding used during data acquisition and analysis. If blinding was not possible, describe why OR explain why blinding was not relevant to your study.   |

Did the study involve field work? ☐ Yes ☐ No

## Field work, collection and transport

|                        |   |
|------------------------|---|
| Field conditions       | <i>Describe the study conditions for field work, providing relevant parameters (e.g. temperature, rainfall).</i>  |
| Location               | <i>State the location of the sampling or experiment, providing relevant parameters (e.g. latitude and longitude, elevation, water depth).</i>   |
| Access & import/export | <i>Describe the efforts you have made to access habitats and to collect and import/export your samples in a responsible manner and in compliance with local, national and international laws, noting any permits that were obtained (give the name of the issuing authority, the date of issue, and any identifying information).</i> |
| Disturbance            | <i>Describe any disturbance caused by the study and how it was minimized.</i>   |

## Reporting for specific materials, systems and methods

We require information from authors about some types of materials, experimental systems and methods used in many studies. Here, indicate whether each material, system or method listed is relevant to your study. If you are not sure if a list item applies to your research, read the appropriate section before selecting a response.

### Materials & experimental systems

|                                     |  |
|-------------------------------------|--|
| n/a                                 | Involved in the study                                  |
| <input checked="" type="checkbox"/> | <input type="checkbox"/> Antibodies                    |
| <input checked="" type="checkbox"/> | <input type="checkbox"/> Eukaryotic cell lines         |
| <input checked="" type="checkbox"/> | <input type="checkbox"/> Palaeontology and archaeology |
| <input checked="" type="checkbox"/> | <input type="checkbox"/> Animals and other organisms   |
| <input checked="" type="checkbox"/> | <input type="checkbox"/> Clinical data                 |
| <input checked="" type="checkbox"/> | <input type="checkbox"/> Dual use research of concern  |
| <input checked="" type="checkbox"/> | <input type="checkbox"/> Plants                        |

### Methods

|                                     |   |
|-------------------------------------|---|
| n/a                                 | Involved in the study                           |
| <input checked="" type="checkbox"/> | <input type="checkbox"/> ChIP-seq               |
| <input checked="" type="checkbox"/> | <input type="checkbox"/> Flow cytometry         |
| <input checked="" type="checkbox"/> | <input type="checkbox"/> MRI-based neuroimaging |

## Antibodies

|                 |   |
|-----------------|---|
| Antibodies used | <i>Describe all antibodies used in the study; as applicable, provide supplier name, catalog number, clone name, and lot number.</i>   |
| Validation      | <i>Describe the validation of each primary antibody for the species and application, noting any validation statements on the manufacturer's website, relevant citations, antibody profiles in online databases, or data provided in the manuscript.</i> |

## Eukaryotic cell lines

Policy information about [cell lines and Sex and Gender in Research](#)

|  |  |
|--|--|
| Cell line source(s)  | <i>State the source of each cell line used and the sex of all primary cell lines and cells derived from human participants or vertebrate models.</i>   |
| Authentication   | <i>Describe the authentication procedures for each cell line used OR declare that none of the cell lines used were authenticated.</i>  |
| Mycoplasma contamination   | <i>Confirm that all cell lines tested negative for mycoplasma contamination OR describe the results of the testing for mycoplasma contamination OR declare that the cell lines were not tested for mycoplasma contamination.</i> |
| Commonly misidentified lines<br>(See <a href="#">ICLAC</a> register) | <i>Name any commonly misidentified cell lines used in the study and provide a rationale for their use.</i>   |

## Palaeontology and Archaeology

|                     |  |
|---------------------|--|
| Specimen provenance | <i>Provide provenance information for specimens and describe permits that were obtained for the work (including the name of the issuing authority, the date of issue, and any identifying information). Permits should encompass collection and, where applicable, export.</i> |
| Specimen deposition | <i>Indicate where the specimens have been deposited to permit free access by other researchers.</i>  |

## Dating methods

If new dates are provided, describe how they were obtained (e.g. collection, storage, sample pretreatment and measurement), where they were obtained (i.e. lab name), the calibration program and the protocol for quality assurance OR state that no new dates are provided.

☐ Tick this box to confirm that the raw and calibrated dates are available in the paper or in Supplementary Information.

## Ethics oversight

Identify the organization(s) that approved or provided guidance on the study protocol, OR state that no ethical approval or guidance was required and explain why not.

Note that full information on the approval of the study protocol must also be provided in the manuscript.

## Animals and other research organisms

Policy information about [studies involving animals](#); [ARRIVE guidelines](#) recommended for reporting animal research, and [Sex and Gender in Research](#)

## Laboratory animals

For laboratory animals, report species, strain and age OR state that the study did not involve laboratory animals.

## Wild animals

Provide details on animals observed in or captured in the field; report species and age where possible. Describe how animals were caught and transported and what happened to captive animals after the study (if killed, explain why and describe method; if released, say where and when) OR state that the study did not involve wild animals.

## Reporting on sex

Indicate if findings apply to only one sex; describe whether sex was considered in study design, methods used for assigning sex. Provide data disaggregated for sex where this information has been collected in the source data as appropriate; provide overall numbers in this Reporting Summary. Please state if this information has not been collected. Report sex-based analyses where performed, justify reasons for lack of sex-based analysis.

## Field-collected samples

For laboratory work with field-collected samples, describe all relevant parameters such as housing, maintenance, temperature, photoperiod and end-of-experiment protocol OR state that the study did not involve samples collected from the field.

## Ethics oversight

Identify the organization(s) that approved or provided guidance on the study protocol, OR state that no ethical approval or guidance was required and explain why not.

Note that full information on the approval of the study protocol must also be provided in the manuscript.

## Clinical data

Policy information about [clinical studies](#)

All manuscripts should comply with the ICMJE [guidelines for publication of clinical research](#) and a completed [CONSORT checklist](#) must be included with all submissions.

## Clinical trial registration

Provide the trial registration number from ClinicalTrials.gov or an equivalent agency.

## Study protocol

Note where the full trial protocol can be accessed OR if not available, explain why.

## Data collection

Describe the settings and locales of data collection, noting the time periods of recruitment and data collection.

## Outcomes

Describe how you pre-defined primary and secondary outcome measures and how you assessed these measures.

## Dual use research of concern

Policy information about [dual use research of concern](#)

### Hazards

Could the accidental, deliberate or reckless misuse of agents or technologies generated in the work, or the application of information presented in the manuscript, pose a threat to:

| No                       | Yes                      |                            |
|--------------------------|--------------------------|----------------------------|
| <input type="checkbox"/> | <input type="checkbox"/> | Public health              |
| <input type="checkbox"/> | <input type="checkbox"/> | National security          |
| <input type="checkbox"/> | <input type="checkbox"/> | Crops and/or livestock     |
| <input type="checkbox"/> | <input type="checkbox"/> | Ecosystems                 |
| <input type="checkbox"/> | <input type="checkbox"/> | Any other significant area |

## Experiments of concern

Does the work involve any of these experiments of concern:

| No                       | Yes  |
|--------------------------|--|
| <input type="checkbox"/> | <input type="checkbox"/> Demonstrate how to render a vaccine ineffective                             |
| <input type="checkbox"/> | <input type="checkbox"/> Confer resistance to therapeutically useful antibiotics or antiviral agents |
| <input type="checkbox"/> | <input type="checkbox"/> Enhance the virulence of a pathogen or render a nonpathogen virulent        |
| <input type="checkbox"/> | <input type="checkbox"/> Increase transmissibility of a pathogen                                     |
| <input type="checkbox"/> | <input type="checkbox"/> Alter the host range of a pathogen  |
| <input type="checkbox"/> | <input type="checkbox"/> Enable evasion of diagnostic/detection modalities                           |
| <input type="checkbox"/> | <input type="checkbox"/> Enable the weaponization of a biological agent or toxin                     |
| <input type="checkbox"/> | <input type="checkbox"/> Any other potentially harmful combination of experiments and agents         |

## Plants

|                       |   |
|-----------------------|---|
| Seed stocks           | Report on the source of all seed stocks or other plant material used. If applicable, state the seed stock centre and catalogue number. If plant specimens were collected from the field, describe the collection location, date and sampling procedures.  |
| Novel plant genotypes | Describe the methods by which all novel plant genotypes were produced. This includes those generated by transgenic approaches, gene editing, chemical/radiation-based mutagenesis and hybridization. For transgenic lines, describe the transformation method, the number of independent lines analyzed and the generation upon which experiments were performed. For gene-edited lines, describe the editor used, the endogenous sequence targeted for editing, the targeting guide RNA sequence (if applicable) and how the editor was applied. |
| Authentication        | Describe any authentication procedures for each seed stock used or novel genotype generated. Describe any experiments used to assess the effect of a mutation and, where applicable, how potential secondary effects (e.g. second site T-DNA insertions, mosaicism, off-target gene editing) were examined.   |

## ChIP-seq

### Data deposition

- ☐ Confirm that both raw and final processed data have been deposited in a public database such as [GEO](#).
- ☐ Confirm that you have deposited or provided access to graph files (e.g. BED files) for the called peaks.

|  |   |
|--|---|
| Data access links<br><i>May remain private before publication.</i> | For "Initial submission" or "Revised version" documents, provide reviewer access links. For your "Final submission" document, provide a link to the deposited data.   |
| Files in database submission                                       | Provide a list of all files available in the database submission.   |
| Genome browser session<br>(e.g. <a href="#">UCSC</a> )             | Provide a link to an anonymized genome browser session for "Initial submission" and "Revised version" documents only, to enable peer review. Write "no longer applicable" for "Final submission" documents. |

### Methodology

|                         |   |
|-------------------------|---|
| Replicates              | Describe the experimental replicates, specifying number, type and replicate agreement.  |
| Sequencing depth        | Describe the sequencing depth for each experiment, providing the total number of reads, uniquely mapped reads, length of reads and whether they were paired- or single-end. |
| Antibodies              | Describe the antibodies used for the ChIP-seq experiments; as applicable, provide supplier name, catalog number, clone name, and lot number.                                |
| Peak calling parameters | Specify the command line program and parameters used for read mapping and peak calling, including the ChIP, control and index files used.                                   |
| Data quality            | Describe the methods used to ensure data quality in full detail, including how many peaks are at FDR 5% and above 5-fold enrichment.  |
| Software                | Describe the software used to collect and analyze the ChIP-seq data. For custom code that has been deposited into a community repository, provide accession details.        |

## Flow Cytometry

### Plots

Confirm that:

- ☐ The axis labels state the marker and fluorochrome used (e.g. CD4-FITC).
- ☐ The axis scales are clearly visible. Include numbers along axes only for bottom left plot of group (a 'group' is an analysis of identical markers).
- ☐ All plots are contour plots with outliers or pseudocolor plots.
- ☐ A numerical value for number of cells or percentage (with statistics) is provided.

### Methodology

Sample preparation

*Describe the sample preparation, detailing the biological source of the cells and any tissue processing steps used.*

Instrument

*Identify the instrument used for data collection, specifying make and model number.*

Software

*Describe the software used to collect and analyze the flow cytometry data. For custom code that has been deposited into a community repository, provide accession details.*

Cell population abundance

*Describe the abundance of the relevant cell populations within post-sort fractions, providing details on the purity of the samples and how it was determined.*

Gating strategy

*Describe the gating strategy used for all relevant experiments, specifying the preliminary FSC/SSC gates of the starting cell population, indicating where boundaries between "positive" and "negative" staining cell populations are defined.*

- ☐ Tick this box to confirm that a figure exemplifying the gating strategy is provided in the Supplementary Information.

## Magnetic resonance imaging

### Experimental design

Design type

*Indicate task or resting state; event-related or block design.*

Design specifications

*Specify the number of blocks, trials or experimental units per session and/or subject, and specify the length of each trial or block (if trials are blocked) and interval between trials.*

Behavioral performance measures

*State number and/or type of variables recorded (e.g. correct button press, response time) and what statistics were used to establish that the subjects were performing the task as expected (e.g. mean, range, and/or standard deviation across subjects).*

### Acquisition

Imaging type(s)

*Specify: functional, structural, diffusion, perfusion.*

Field strength

*Specify in Tesla*

Sequence & imaging parameters

*Specify the pulse sequence type (gradient echo, spin echo, etc.), imaging type (EPI, spiral, etc.), field of view, matrix size, slice thickness, orientation and TE/TR/flip angle.*

Area of acquisition

*State whether a whole brain scan was used OR define the area of acquisition, describing how the region was determined.*

Diffusion MRI

☐ Used

☐ Not used

### Preprocessing

Preprocessing software

*Provide detail on software version and revision number and on specific parameters (model/functions, brain extraction, segmentation, smoothing kernel size, etc.).*

Normalization

*If data were normalized/standardized, describe the approach(es): specify linear or non-linear and define image types used for transformation OR indicate that data were not normalized and explain rationale for lack of normalization.*

Normalization template

*Describe the template used for normalization/transformation, specifying subject space or group standardized space (e.g. original Talairach, MNI305, ICBM152) OR indicate that the data were not normalized.*

Noise and artifact removal

*Describe your procedure(s) for artifact and structured noise removal, specifying motion parameters, tissue signals and physiological signals (heart rate, respiration).*

Volume censoring

*Define your software and/or method and criteria for volume censoring, and state the extent of such censoring.*

## Statistical modeling & inference

Model type and settings

*Specify type (mass univariate, multivariate, RSA, predictive, etc.) and describe essential details of the model at the first and second levels (e.g. fixed, random or mixed effects; drift or auto-correlation).*

Effect(s) tested

*Define precise effect in terms of the task or stimulus conditions instead of psychological concepts and indicate whether ANOVA or factorial designs were used.*

Specify type of analysis: ☐ Whole brain ☐ ROI-based ☐ Both

Statistic type for inference

*Specify voxel-wise or cluster-wise and report all relevant parameters for cluster-wise methods.*

(See [Eklund et al. 2016](#))

Correction

*Describe the type of correction and how it is obtained for multiple comparisons (e.g. FWE, FDR, permutation or Monte Carlo).*

## Models & analysis

n/a | Involved in the study

☐ ☐ Functional and/or effective connectivity

☐ ☐ Graph analysis

☐ ☐ Multivariate modeling or predictive analysis

Functional and/or effective connectivity

*Report the measures of dependence used and the model details (e.g. Pearson correlation, partial correlation, mutual information).*

Graph analysis

*Report the dependent variable and connectivity measure, specifying weighted graph or binarized graph, subject- or group-level, and the global and/or node summaries used (e.g. clustering coefficient, efficiency, etc.).*

Multivariate modeling and predictive analysis

*Specify independent variables, features extraction and dimension reduction, model, training and evaluation metrics.*

# Selective silencing of antibiotic-tethered ribosomes as a resistance mechanism against aminoglycosides

Corresponding Author: Dr Ingo Wohlgemuth

This file contains all reviewer reports in order by version, followed by all author rebuttals in order by version.

Version 0:

Reviewer comments:

Reviewer #1

(Remarks to the Author)

In this elegant study, Ghosh Dastidar et al. investigate how mutations in *fusA*, the gene coding for EF-G, confer resistance to aminoglycoside antibiotics. Using a combination of quantitative mass spectrometry, kinetic analyses, cryo-EM and live-cell imaging, the authors propose a mechanism by which *fusA* mutations selectively slow down elongation by drug-bound ribosomes. Although bacterial growth is only mildly affected by the mutations, the drug has more time to dissociate from the ribosome, resulting in fewer aminoglycoside-induced miscoding errors and decreased production of aberrant proteins compared to wild-type cells. This, in turn, preserves membrane integrity and prevents the self-promoted aminoglycoside uptake normally observed for this family of antibiotics, leading to resistance.

The identification of this novel resistance mechanism, termed “selective silencing of corrupted targets” is an important step forward in our understanding of antibiotic action and resistance. The study is well-designed, the conclusions are fully supported by the available data, and the results will be of interest to both the antibiotic resistance and translation fields.

Consequently, I only have the following minor comments for the authors to address:

- Lines 116-118. According to Fig. 1C, the extents of resistance to Nea and Neo appear to be very similar, even though error bars for Nea are larger. However the authors claim that the *fusA* mutant gives resistance to Neo (which induces error clusters), but not to Nea (which does not induce error clusters). This point should be clarified.
- Fig. 1b. The difference between the MG1655 and wt strains is explained in Supp. Fig. 3 and in the Methods section, but it would also be helpful to include this explanation on p. 4.
- Lines 244-251. It would be helpful to mention here that the structure obtained in this study was compared to an earlier structure that also contains Apr (Ref. 46). At present, this point is unclear and gives the impression that the Apr and EF-G P610L-containing structure is being compared to an EF-G wt structure lacking the drug.
- Fig. 3. Densities for the drug and for Domain IV of EF-G should be shown as supplementary figures. What changes (if any) does the mutation induce in EF-G?
- Line 333. Delete “the of”.
- Lines 366-381. How were specific mutation pairs chosen? Is the focus only on the most abundant peptides? In any case, the methodology should be briefly explained in the main text.
- Lines 345-346. Please specify the range of concentrations that “high Apr concentration” refers to.
- Line 448. The text should read “in the absence or presence of”.

Reviewer #2

(Remarks to the Author)

The work of Dastidar, Freyer, et al. presents a model to explain a resistance phenotype for aminoglycoside antibiotics (AGAs) whose mechanism had remained mysterious. Interpretation of the current data is based on previous work by the same group (Wohlgemuth et al, 2021) where it was elucidated that miscoding caused by AGAs results in translating proteins with clusters of erroneous amino acids, leading to proteotoxic stress and cell death. Here, based on compelling experimental evidence, authors propose how a bad trait, mutations in the EF-G encoding gene *fusA*, ends up being advantageous for AGA poisoned cells: the more sluggish AGA-bound ribosomes where translocation is driven by mutant EF-G, produce proteins with less error clusters and therefore, the proteome remains reasonably healthy and the membranes robust. The paper is clearly written, well-organized and the work is conceptually significant, using basic principles of translation to explain resistance to clinically-important antibiotics.

The following points of critique are mainly aimed to address specific points which are not clear in the manuscript:

- Fig. 1a: it won't be clear for many non-expert readers which portion of the ribosome is shown. Adding a panel with an overview of the whole AGA-bound ribosome interacting with EF-G and better color coding would help.
- Supplementary Fig. 2: the cartoon for the Gain of Function Model 4 is confusing as it shows that the translation aided by EF-G variants would result in proteins with more error clusters. How would this lead to resistance?
- Text is missing an explanation of the particles distribution shown in the bar graph of Fig. 3e and Supplementary Fig. 6 to clarify how the conclusions of which step is inhibited have been actually drawn.
- Related to the point above, legend of Fig. 3d: "in EF-G P610L the key reaction of Pi release is slowed down, inhibiting the conformational rearrangement required to promote the tRNA movement into the CHI state" – where does this come from?— from particle distribution shown in 3e?
- Fig. 3e: requires a comparison of the distribution of the same states but in the absence of Apr.
- It is not clear why mutant EF-G inhibits formation of the CHI state when AG is present
- The sentence in lane 285, "This contradicts the 'gain of function model'..." needs a better explanation.
- Ln 327-328- experiments assess relative error cluster formation, not rate of translation speed.
- p.11- Are the off rates of AGs bound to the translating ribosome known? If yes, is the model compatible with those rates?
- Would expression of wt EF-G overcome AGA resistance of the strains with mutations in chromosomal *fusA*?

Minor points:

- Revise the sentence on lanes 71-73: "...mutations...can confer high-level resistance, their impact on... resistance is limited..."
- ref. to Supplementary Fig. 2 in lanes 94-96 is misplaced.
- Lane 333, delete "of the".
- Lane 371, "than" not "that".
- Ln 436, correct "First, we first..."

Reviewer #3

(Remarks to the Author)

The manuscript by Dastidar et al. reports the results of an original integrative study poised at unraveling a new antibiotic resistance mechanism, which neutralizes the action of several aminoglycosides (AGAs), through certain mutations in the EF-G gene, *fusA*. The authors show that EF-G resistance variants slow ribosome movement along mRNA when aminoglycosides are bound in a selective fashion. The delay resulting from the slowing down increases the chance that the drug dissociates before misreading occurs.

The authors found that *fusA* mutations confer resistance early in treatment by preventing self-promoted aminoglycoside uptake, which occurs consequently to the accumulation of misreading errors on the translated membrane proteins/transporters.

Indeed, the accumulation of faulty membrane proteins and misreading-induced metabolic by-products makes the inner membrane permeable to AGAs. As more and more AGAs enter the cell, more ribosomes bind AGAs and become corrupted. Over time, this self-promoted uptake leads to a massive influx of AGAs, resulting in a burst of translation errors leading ultimately to the damage of macromolecular structures, the disruption of the general metabolism and the membrane voltage dysregulation, all leading to cell death.

AGA resistance has been greatly characterized over the past decades and most AGA resistance mutations occur outside of the ribosome itself. Unexpectedly, a major hotspot of AGA resistance mutations is the *fusA* gene. Interestingly, *fusA* mutations confer resistance in various bacteria as well as in parasites such as *Leishmania*.

Despite their clinical relevance, the mechanism by which *fusA* mutations confer resistance remained thus far unclear, as EF-G neither blocks AGA binding nor contacts the decoding center.

The authors successfully demonstrate the existence of this previously unrecognized resistance mechanism that selectively silences corrupted targets, by applying a combination of quantitative mass spectrometry (MS), live-cell imaging, kinetic analysis, and cryo-EM, thus revealing a novel AGAs resistance strategy with potential therapeutic implications.

The authors found that *fusA* mutations specifically counteract the effects of certain AGAs that both disrupt translocation and induce misreading with error cluster formation.

The authors focused on three mutations in domain IV of EF-G (F593L, A608E and P610L). First, Dastidar et al. show that the proteomic changes induced by these mutations were minimal. They have analyzed the in-vitro translocation activity of the purified EF-G variants in the absence of AGAs and show that translocation rates substantially decreased in the presence of AGAs, supporting the idea that these mutants are selectively hindered in promoting translocation on AGA-bound ribosomes

The authors went on and probed the structure of an EF-G variant (P610L) in complex with the ribosome and Apramycin (Apr), using single-particle cryo-EM. The resulting structure superimposes nearly perfectly with EF-G wt and shows no significant structural changes in the decoding center or the drug-binding site, supporting the notion that EF-G variants do not displace the drug from the ribosome. They also show that the early stages of translocation up to GTP hydrolysis are unaffected by Apr but the later steps appear to be inhibited, particularly Pi release and the tRNA movement into chimeric states.

In summary, the authors show that fusA mutations silence AGA-bound ribosomes, preserving membrane integrity, and attenuating AGA uptake. This strategy minimizes translation errors without modifying the ribosome itself.

The manuscript is well written and the figures are clear. The references are sufficient, as far as the reviewer could tell and the performed experiments are state of the art. Furthermore, the depth of the performed analysis is simply overwhelming.

The reviewer has no major points to raise and only has very few minor comments. The manuscript can be in principle accepted in its current state.

Minor comments

Line 168 "these adaptations are likely due to changes in translation rates"

AdaptATions, not adaptations

Why was SlyD used as an in-vitro translation model? Why not other mRNAs?

Figure 3 a-c:

Could the lack of significant changes in Apr binding on EF-G associated ribosomes, between the wt and the EF-G variant/mutant, rather be a consequence of the relatively modest resolution of the cryo-EM? Indeed, at 3Å many details can't be interpreted, such as solvent molecules and other subtle conformational changes with certainty...

Also, why is the resolution relatively modest at a time where structures of bacterial ribosomes are frequently below 2Å?

Why was Apramycin used or considered as the archetype AGA?

In cases where reviewers are anonymous, credit should be given to 'Anonymous Referee' and the source. The images or other third party material in this Peer Review File are included in the article's Creative Commons license, unless indicated otherwise in a credit line to the material. If material is not included in the article's Creative Commons license and your intended use is not permitted by statutory regulation or exceeds the permitted use, you will need to obtain permission directly from the copyright holder. To view a copy of this license, visit <https://creativecommons.org/licenses/by/4.0/>

## Reviewer #1 (Remarks to the Author):

In this elegant study, Ghosh Dastidar et al. investigate how mutations in *fusA*, the gene coding for EF-G, confer resistance to aminoglycoside antibiotics. Using a combination of quantitative mass spectrometry, kinetic analyses, cryo-EM and live-cell imaging, the authors propose a mechanism by which *fusA* mutations selectively slow down elongation by drug-bound ribosomes. Although bacterial growth is only mildly affected by the mutations, the drug has more time to dissociate from the ribosome, resulting in fewer aminoglycoside-induced miscoding errors and decreased production of aberrant proteins compared to wild-type cells. This, in turn, preserves membrane integrity and prevents the self-promoted aminoglycoside uptake normally observed for this family of antibiotics, leading to resistance.

The identification of this novel resistance mechanism, termed “selective silencing of corrupted targets” is an important step forward in our understanding of antibiotic action and resistance. The study is well-designed, the conclusions are fully supported by the available data, and the results will be of interest to both the antibiotic resistance and translation fields.

Reply: We thank the reviewer for the positive feedback on our manuscript and helpful comments.

Consequently, I only have the following minor comments for the authors to address:

- Lines 116-118. According to Fig. 1C, the extents of resistance to Nea and Neo appear to be very similar, even though error bars for Nea are larger. However the authors claim that the *fusA* mutant gives resistance to Neo (which induces error clusters), but not to Nea (which does not induce error clusters). This point should be clarified.

Reply: As stated in the main text (lines 117-119 of the revised manuscript), the *fusA* mutations do not confer significant resistance to Nea. While the effect size appears similar to Neo, only the effect of Neo is statistically significant. For Nea, even after increasing the number of biological replicates to  $n=15$ , the effect remained statistically non-significant.

- Fig. 1b. The difference between the MG1655 and wt strains is explained in Supp. Fig. 3 and in the Methods section, but it would also be helpful to include this explanation on p. 4.

Reply: Done. We included additional information on the wt strain into the main text (l. 101-105) and refer to the Method sections for the details on cloning strategy (the addition is marked red):

“To explore how *fusA* mutations confer resistance to AGAs, we constructed *E. coli* MG1655 strains harboring three frequently reported laboratory-evolved EF-G variants (F593L, A608E, and P610L) (Fig. 1a), which belong to a prominent cluster of resistance mutations in EF-G domain IV (Supplementary Data 1), **along with an isogenic wild-type control generated by the same cloning strategy but retaining the wt sequence** (see Methods, Supplementary Fig. 3a-d)”.

- Lines 244-251. It would be helpful to mention here that the structure obtained in this study was compared to an earlier structure that also contains Apr (Ref. 46). At present, this point is unclear

and gives the impression that the Apr and EF-G P610L-containing structure is being compared to an EF-G wt structure lacking the drug.

Reply: Done (l. 204-206). “Superimposing the Apr-bound ribosome-EF-G P610L complex with the previously published Apr-bound ribosome EF-G wt complex <sup>51</sup> shows no significant structural changes in the decoding center or drug-binding site (Fig. 3c).”

- Fig. 3. Densities for the drug and for Domain IV of EF-G should be shown as supplementary figures. What changes (if any) does the mutation induce in EF-G?

Reply: Done. In response to the reviewer’s and editor’s comments, Supplementary Fig. 6 has been split into two, with biological aspects shown in Supplementary Fig. 6, while technical aspects are presented in Supplementary Fig. 10). Densities for the drug (Supplementary Fig. 6b) and for domain IV of EF-G (Fig S6d) have been added. The overall cryo-EM densities for EF-G in H1 and H2 states show no significant differences between mutant (present study) and wt EF-G (Petrychenko et al. Nat Commun 2021). Domain IV is dynamic in all structures, as described in detail in the published paper. As the P610L mutation is located in the hinge region between domains IV and III/V of EF-G, we performed extensive sorting of this area, but could not detect clear differences in domain IV dynamics.

- Line 333. Delete “the of”.

Reply: Done (l. 254), thank you.

- Lines 366-381. How were specific mutation pairs chosen? Is the focus only on the most abundant peptides? In any case, the methodology should be briefly explained in the main text.

Reply: We agree that the details of error cluster analysis may not be fully clear from the main text (l. 242-270 of the revised manuscript). However, to maintain readability for a general audience, we prefer not to include extensive methods details in the Results section and instead refer readers to the Methods. In the revised Methods, we have rephrased the selection procedure to make it more specific and transparent, ensuring that the key aspects are now clearly traceable (l. 736-741):

“From the list of all possible peptides with error clusters, we prioritized missense peptides with good ionizability and observability to ensure a suitable dynamic range of detection for analyzing error cluster reduction in *fusA* mutant strains. To enable reproducible quantification, we selected peptides with moderate hydrophobicity and good chemical stability. Furthermore, we chose missense peptides with amino acid substitutions that did not substantially destabilize EF-Tu and varied in the distance between individual misreading events.”

- Lines 345-346. Please specify the range of concentrations that “high Apr concentration” refers to.

Reply: The term “high” was meant to refer here to all concentrations above which the error burden decreases again because the cells die faster than they can synthesize large quantities of defective proteins. In order to avoid the evaluative term “high,” we have now specified the exact

concentration range (l. 1197-1198): “The apparently lower error frequency in wt cells at high Apr concentrations  $\geq 32\mu\text{M}$  is due to massive cell death and the rapid decline in actively growing cells.”

- Line 448. The text should read “in the absence or presence of”.

Reply: Done, thank you.

## **Reviewer #2 (Remarks to the Author):**

The work of Dastidar, Freyer, et al. presents a model to explain a resistance phenotype for aminoglycoside antibiotics (AGAs) whose mechanism had remained mysterious. Interpretation of the current data is based on previous work by the same group (Wohlgemuth et al, 2021) where it was elucidated that miscoding caused by AGAs results in translating proteins with clusters of erroneous amino acids, leading to proteotoxic stress and cell death. Here, based on compelling experimental evidence, authors propose how a bad trait, mutations in the EF-G encoding gene *fusA*, ends up being advantageous for AGA poisoned cells: the more sluggish AGA-bound ribosomes where translocation is driven by mutant EF-G, produce proteins with less error clusters and therefore, the proteome remains reasonably healthy and the membranes robust. The paper is clearly written, well-organized and the work is conceptually significant, using basic principles of translation to explain resistance to clinically-important antibiotics.

Reply: We thank the reviewer for positive comments and appreciating the significance of the work.

The following points of critique are mainly aimed to address specific points which are not clear in the manuscript:

- Fig. 1a: it won't be clear for many non-expert readers which portion of the ribosome is shown. Adding a panel with an overview of the whole AGA-bound ribosome interacting with EF-G and better color coding would help.

Reply: We thank the reviewer for the suggestion and added the view of the complete ribosome with two tRNAs and EF-G in Figure 1a. The color scheme for tRNAs and EF-G has been harmonized with the rest of the manuscript.

- Supplementary Fig. 2: the cartoon for the Gain of Function Model 4 is confusing as it shows that the translation aided by EF-G variants would result in proteins with more error clusters. How would this lead to resistance?

Reply: The gain of function mechanism was proposed before error clusters were identified. We agree that Model 4, as originally illustrated, appears unlikely and would in fact lead to accumulation of error clusters. However, for the sake of completeness in our literature overview, we would like to keep the model. To present it in a more neutral way, we have revised the schematic and removed the strong error cluster formation.

- Text is missing an explanation of the particles distribution shown in the bar graph of Fig. 3e and Supplementary Fig. 6 to clarify how the conclusions of which step is inhibited have been actually drawn.

Reply: We now added an explanation in the text (now p. 6-7): “With EF-G P610L, we could not detect any particles in the chimeric state, despite extensive sorting of the cryo-EM data (Methods). Furthermore, we could also not find any post-Pi-release state that would correspond to a tRNA hybrid state with EF-G-GDP bound, as we found previously for wt EF-G<sup>51</sup>. Accordingly, with EF-G P610L the early stages of translocation up to GTP hydrolysis are unaffected by Apr but the later steps appear to be inhibited, particularly Pi release and the tRNA movement into chimeric states.”

- Related to the point above, legend of Fig. 3d: “in EF-G P610L the key reaction of Pi release is slowed down, inhibiting the conformational rearrangement required to promote the tRNA movement into the CHI state” – where does this come from?—from particle distribution shown in 3e?

Reply: Yes, please refer to previous point.

- Fig. 3e: requires a comparison of the distribution of the same states but in the absence of Apr.

Reply: In the present manuscript, we focus specifically on the impact of EF-G mutations on the particle distribution in the presence of Apr, and did not acquire cryo-EM data in the absence of Apr. Such experiments would be beyond the scope of the present manuscript, because in the absence of AGA, these EF-G mutants promote complete translocation at a rate comparable to that of wt EF-G (i.e., in milliseconds-seconds range), which makes cryo-EM experiments extremely tedious.

- It is not clear why mutant EF-G inhibits formation of the CHI state when AG is present

Reply: That is correct – our cryo-EM data clearly show that mutant EF-G blocks CHI state formation in the presence of AGA, but we do not yet understand the underlying mechanism. AGA binding to the ribosome greatly increases the energy barrier of translocation, possibly by reducing the dynamics of the decoding center. A further impairment of EF-G dynamics caused by mutation could uncouple ribosome and EF-G movements. At present, however, these remain speculative considerations that lead beyond the resistance focus of this paper, and we would prefer not to expand on them here.

- The sentence in lane 285, “This contradicts the ‘gain of function model’ ...” needs a better explanation.

Reply: We thank the reviewer for this suggestion. We now more explicitly write (l. 218-220): “The fact that EF-G P610L and Apr can bind simultaneously, and that the mutation impairs late translocation steps is inconsistent with a ‘gain-of-function’ model (Supplementary Fig. 2, model

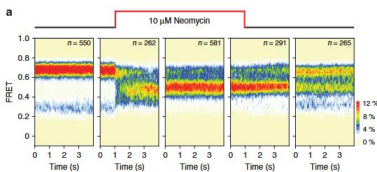
4). Together with the kinetic analysis (Fig. 2), these results demonstrate that EF-G variants are impaired in facilitating translation on AGA-bound ribosomes.”

- Ln 327-328- experiments assess relative error cluster formation, not rate of translation speed.

Reply: This is correct, thanks for pointing that out. Error cluster formation and its distance dependence provide indirect information on the residual speed of AGA-bound ribosomes, but do not allow a direct determination of translation rates as long as off rates for AGAs are not established. However, as we write in l. 244-247, “..., selective silencing of AGA-bound ribosomes in *fusA* mutant strains increases the chance that AGA will dissociate from the ribosome before several elongation cycles are completed, thereby suppressing error cluster formation.” We have revised the following sentence to read (l. 247-249): “**To assess whether translation proceeds slow enough for AGA to dissociate before multiple elongation cycles are completed**, we measured error cluster formation in wt and mutant strains in vivo using targeted MS. “

- p.11- Are the off rates of AGs bound to the translating ribosome known? If yes, is the model compatible with those rates?

Reply: To the best of our knowledge, the dissociation rate constants of AGAs from the ribosome have not been determined. While MICs, IC<sub>50</sub> and K<sub>d</sub> values are well established, no quantitative assay currently exists that directly yields k<sub>off</sub> values. Single-molecule-rinse-out experiments indicate that dissociation occurs at the time scale of seconds (Wasserman et al., 2015), which is qualitatively consistent with our model. For more quantitative comparisons, the k<sub>off</sub> rates as well as the translation rates of AGA-bound ribosomes at low AGA concentrations (at high conc. often multiple binding sites are occupied) would need to be established, which is beyond the scope of this work.



- Would expression of wt EF-G overcome AGA resistance of the strains with mutations in chromosomal *fusA*?

Reply: Yes, there are examples in the literature showing that the resistance was reverted by complementing the *fusA* mutant strain with wild-type EF-G. We cite Ibacache-Quiroga et al. (2018) and Maunders et al. (2020) as examples in lines 92–93.

Minor points:

- Revise the sentence on lines 71-73: “...mutations...can confer high-level resistance, their impact on... resistance is limited...”

Reply: Thank you, we edited the sentence, and it now reads: “**Although 16S rRNA mutations in the ribosomal decoding center can confer high-level resistance, their impact is limited because most pathogens have multiple rRNA-encoding genes, so acquiring mutations in all copies simultaneously is unlikely**”.

- ref. to Supplementary Fig. 2 in lanes 94-96 is misplaced.

Reply: Changed as requested; the sentence now refers to Figure 1 and reads as follows: “Despite their clinical relevance, the mechanism by which *fusA* mutations confer resistance remains unclear, as EF-G cannot directly block AGA binding or contact the decoding center (Fig. 1A).”

- Lane 333, delete “of the”.

Reply: Done

-Lane 371, “than” not “that”.

Reply: Done

- Ln 436, correct “First, we first...”

Reply: Done

### **Reviewer #3 (Remarks to the Author):**

The manuscript by Dastidar et al. reports the results of an original integrative study poised at unraveling a new antibiotic resistance mechanism, which neutralizes the action of several aminoglycosides (AGAs), through certain mutations in the EF-G gene, *fusA*. The authors show that EF-G resistance variants slow ribosome movement along mRNA when aminoglycosides are bound in a selective fashion. The delay resulting from the slowing down increases the chance that the drug dissociates before misreading occurs.

The authors found that *fusA* mutations confer resistance early in treatment by preventing self-promoted aminoglycoside uptake, which occurs consequently to the accumulation of misreading errors on the translated membrane proteins/transporters.

Indeed, the accumulation of faulty membrane proteins and misreading-induced metabolic by-products makes the inner membrane permeable to AGAs. As more and more AGAs enter the cell, more ribosomes bind AGAs and become corrupted. Over time, this self-promoted uptake leads to a massive influx of AGAs, resulting in a burst of translation errors leading ultimately to the damage of macromolecular structures, the disruption of the general metabolism and the membrane voltage dysregulation, all leading to cell death.

AGA resistance has been greatly characterized over the past decades and most AGA resistance mutations occur outside of the ribosome itself. Unexpectedly, a major hotspot of AGA resistance mutations is the *fusA* gene. Interestingly, *fusA* mutations confer resistance in various bacteria as well as in parasites such as *Leishmania*.

Despite their clinical relevance, the mechanism by which *fusA* mutations confer resistance remained thus far unclear, as EF-G neither blocks AGA binding nor contacts the decoding center.

The authors successfully demonstrate the existence of this previously unrecognized resistance mechanism that selectively silences corrupted targets, by applying a combination of quantitative mass spectrometry (MS), live-cell imaging, kinetic analysis, and cryo-EM, thus revealing a novel AGAs resistance strategy with potential therapeutic implications.

The authors found that *fusA* mutations specifically counteract the effects of certain AGAs that both disrupt translocation and induce misreading with error cluster formation.

The authors focused on three mutations in domain IV of EF-G (F593L, A608E and P610L).

First, Dastidar et al. show that the proteomic changes induced by these mutations were minimal. They have analyzed the in-vitro translocation activity of the purified EF-G variants in the absence of AGAs and show that translocation rates substantially decreased in the presence of AGAs, supporting the idea that these mutants are selectively hindered in promoting translocation on AGA-bound ribosomes

The authors went on and probed the structure of an EF-G variant (P610L) in complex with the ribosome and Apramycin (Apr), using single-particle cryo-EM. The resulting structure superimposes nearly perfectly with EF-G wt and shows no significant structural changes in the decoding center or the drug-binding site, supporting the notion that EF-G variants do not displace the drug from the ribosome. They also show that the early stages of translocation up to GTP hydrolysis are unaffected by Apr but the later steps appear to be inhibited, particularly Pi release and the tRNA movement into chimeric states.

In summary, the authors show that *fusA* mutations silence AGA-bound ribosomes, preserving membrane integrity, and attenuating AGA uptake. This strategy minimizes translation errors without modifying the ribosome itself.

The manuscript is well written and the figures are clear. The references are sufficient, as far as the reviewer could tell and the performed experiments are state of the art. Furthermore, the depth of the performed analysis is simply overwhelming.

The reviewer has no major points to raise and only has very few minor comments. The manuscript can be in principle accepted in its current state.

[Reply: We thank the reviewer's encouraging remarks and recognition of the contribution of our study.](#)

Minor comments

Line 168 “these adaptations are likely due to changes in translation rates”

AdaptATions, not adaptations

Reply: Thank you for catching this. Done

Why was SlyD used as an in-vitro translation model? Why not other mRNAs?

Reply: We chose *slyD* for two reasons. First, the *in-vitro* translation of *slyD* mRNA is rapid and produces few translation intermediates. This is advantageous, as such intermediates could mask the effects of the EF-G variants under investigation. Second, although less important, SlyD is histidine-rich, which facilitates purification by nickel affinity chromatography if questions about its in-vivo relevance arise. Beyond these points, *slyD* simply serves as one representative model mRNA.

Figure 3 a-c:

Could the lack of significant changes in Apr binding on EF-G associated ribosomes, between the wt and the EF-G variant/mutant, rather be a consequence of the relatively modest resolution of the cryo-EM? Indeed, at 3 Å many details can't be interpreted, such as solvent modelules and other subtle conformational changes with certainty...

Also, why is the resolution relatively modest at a time where structures of bacterial ribosomes are frequently below 2 Å?

Reply: The present resolution of the key states is largely explained by the transient and dynamic nature of ribosome-EF-G complexes investigated here, while ribosome structures below 2 Å usually describe more stable ribosomal states. Our structures show that EF-G mutation changes neither ribosome occupancy with EF-G or AGA, EF-G position, or the AGA interaction network on the ribosome, indicating that potential subtle unresolved differences do not have a significant impact on Apr binding to the ribosome.

Why was Apramycin used or considered as the archetype AGA?

Reply: Apramycin was chosen because it is a promising AGA candidate with markedly reduced ototoxicity compared to currently used AGAs. Additionally, its structure allows to evade many widespread resistance mechanisms. Therefore, it is important to investigate whether established resistance mutations also affect future drug candidates. Furthermore, apramycin is a good representative of its drug class. It shares ring I and II with DOS AGAs, binds to the canonical site in the decoding center, inhibits translocation, induces misreading and error clusters, and is subject to similar cellular resistance mutations.

From a strictly structural perspective, apramycin, with its 4-monosubstituted core, is not the archetype AGA. However, the concept of an “archetype” AGA is heuristic and an archetype AGA is difficult to define, as AGAs can be categorized by structural features, their kinetics on the ribosome, their cellular action, uptake, side effects, or resistance profiles. Given this diversity, we validated key aspects of the proposed mechanism for different AGAs to ensure generality.

## Description of Additional Supplementary Files:

**Supplementary Data 1:** EF-G resistance variants across pathogens: Amino acid substitutions in EF-G from diverse pathogens that evolved under aminoglycoside selection (blue) or were identified in clinical isolates (red). Corresponding aminoglycosides and PubMed references are listed. The sequences are aligned to the EF-G sequence from *E. coli* MG1655.

## Supplementary Information for

### Selective silencing of antibiotic-tethered ribosomes as a resistance mechanism against aminoglycosides

Nilanjan Ghosh Dastidar<sup>1,2, †</sup>, Nicola S. Freyer<sup>1,2, †</sup>, Valentyn Petrychenko<sup>3</sup>, Ana C. de A. P. Schwarzer<sup>3</sup>, Bee-Zen Peng<sup>1</sup>, Ekaterina Samatova<sup>1</sup>, Christina Kothe<sup>1</sup>, Marlen Schmidt<sup>4</sup>, Frank Peske<sup>1</sup>, Antonio Z. Politi<sup>5</sup>, Henning Urlaub<sup>6,7</sup>, Niels Fischer<sup>3</sup>, Marina V. Rodnina<sup>1\*</sup>, Ingo Wohlgemuth<sup>2\*</sup>

<sup>1</sup>Department for Physical Biochemistry, Max Planck Institute for Multidisciplinary Sciences, Göttingen, Germany

<sup>2</sup>Project Group Fidelity of Protein Synthesis in vivo, Department for Physical Biochemistry, Max Planck Institute for Multidisciplinary Sciences, Göttingen, Germany

<sup>3</sup>Project Group Molecular Machines in Motion, Department for Physical Biochemistry, Max Planck Institute for Multidisciplinary Sciences, Göttingen, Germany

<sup>4</sup>Genetic Engineering Heidelberg GmbH, Heidelberg, Germany

<sup>5</sup>Facility for Light Microscopy, Max Planck Institute for Multidisciplinary Sciences, Göttingen, Germany

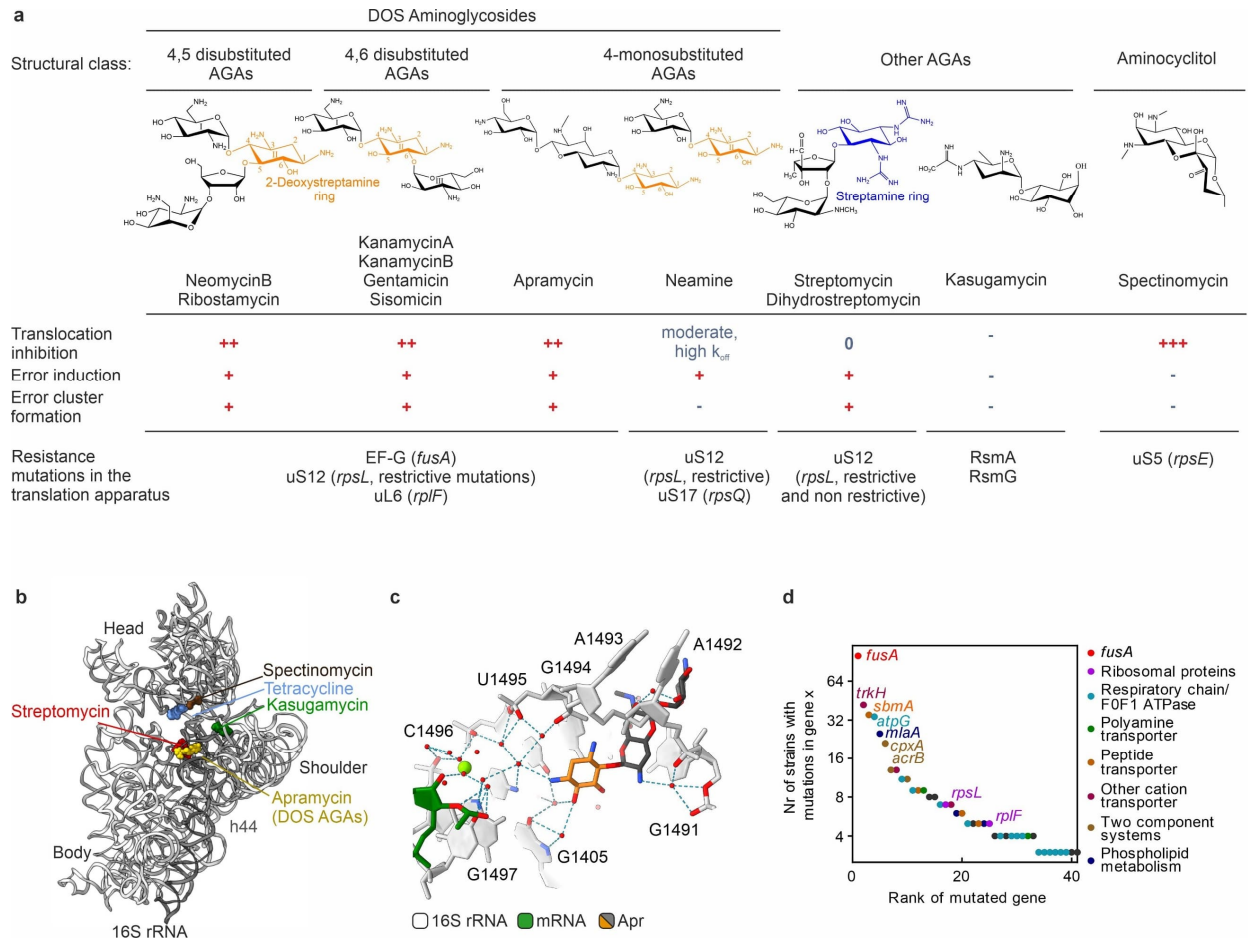
<sup>6</sup>Bioanalytical Mass Spectrometry Group, Max Planck Institute for Multidisciplinary Sciences, Göttingen, Germany

<sup>7</sup>Institute of Clinical Chemistry, Bioanalytics, University Medical Center Göttingen, Göttingen, Germany

<sup>†</sup>These authors contributed equally

\* Correspondence: [Ingo.Wohlgemuth@mpinat.mpg.de](mailto:Ingo.Wohlgemuth@mpinat.mpg.de), [Rodnina@mpinat.mpg.de](mailto:Rodnina@mpinat.mpg.de)

# Supplementary Figures



**Supplementary Figure 1. Action of DOS aminoglycosides on the ribosome, related to Figure 1**

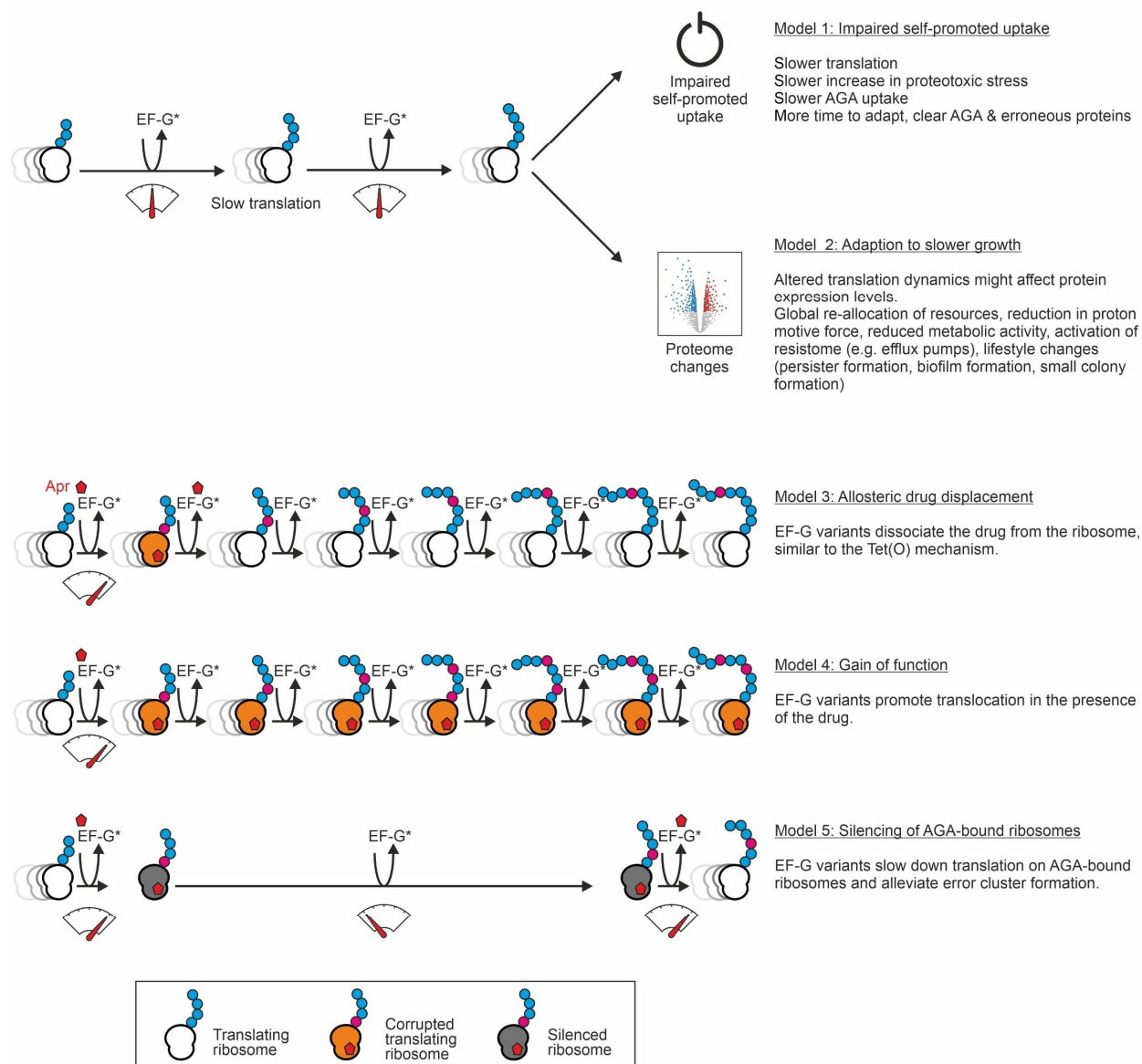
**(a)** Chemical classification of aminoglycoside antibiotics (AGAs). Most AGAs belong to the class of 2-deoxystreptamine (2-DOS) AGAs. Neomycin (Neo) and ribostamycin (Rib) share a 4,5 disubstituted 2-DOS ring (II). Kanamycin (KanA, KanB), gentamicin (Gen) and sisomicin (Sis) belong to the 4,6 disubstituted 2-DOS family, whereas in apramycin (Apr) the 2-DOS ring is monosubstituted at position 4. All these AGAs target helix 44 of 16S rRNA at the decoding center (DC) of the ribosome. They induce misreading, resulting in single errors and error clusters<sup>1</sup>, and slow down tRNA-mRNA translocation. Treatment with DOS AGAs promotes *fusA* (coding for EF-G) resistance mutations in many pathogens<sup>2,3,4,5,6,7,8,9,10,11,12,13,14,15,16,17,18,19,20,21,22,23,24,25,26,27,28,29,30,31,32,33,34,35,36,37,38,39,40,41</sup>. Less frequently, mutations are found in *rpsL* (coding for uS12) and *rplF* (coding for uL6)<sup>42</sup>. Neamine (Nea) is the smallest 2-DOS AGA with only two rings that are necessary to recognize the binding site in the DC. It has a lower affinity to the ribosome<sup>43</sup>, higher Minimal Inhibitory Concentrations (MIC)<sup>44</sup>, and does not promote error cluster formation<sup>1</sup>. Neamine resistance mutations were reported in *rpsL* and *rpsQ* (coding for uS17)<sup>45,46,47</sup>. Streptomycin (Str) and dihydrostreptomycin (Dhs) have a streptamine ring; they induce misreading and error cluster formation<sup>1</sup> but have only a moderate effect on translocation<sup>48</sup> and induce resistance mutations in *rpsL*<sup>12</sup>. Non-restrictive resistance mutations in uS12 prevent drug binding, confer high Str resistance and are associated with moderate fitness costs. In contrast, restrictive *rpsL* mutations confer a higher translation fidelity than the wt but only moderate resistance, and have higher fitness costs.

Kasugamycin (Ksg) is a small, structurally unrelated AGA that inhibits initiation<sup>49</sup> and the transition to elongation in a sequence-dependent manner<sup>50</sup>. Resistance mutations against Ksg are selected in the methyltransferases RsmA and RsmG. Spectinomycin (Spc) is structurally similar to AGAs and belongs to the class of aminocyclitols; it inhibits translocation but has no effect on the decoding fidelity of the ribosome. Spc resistance mutations evolve in *rpsE* (encoding uS5)<sup>12,51,52</sup>. *FusA* mutations confer little or no resistance against Nea, Str or Spc (Figure 1C)<sup>24,53</sup>, consistent with the fact that *fusA* mutations are only selected upon 2-DOS-AGA treatment<sup>12</sup>.

**(b)** Superposition of drug binding sites on the small ribosomal subunit (SSU). Shown is the binding site for Apr (gold) and other 2-DOS AGAs at the top of helix 44 of 16S rRNA (PDB entry 7PJS)<sup>54</sup>. At elevated drug concentrations 2-DOS AGAs can also bind to secondary binding sites, which synergistically inhibits translation<sup>54</sup>. However, because rRNA mutations in helix 44 alone confer high AGA resistance by preventing AGA binding<sup>44</sup>, secondary binding sites are less important for AGA uptake and misreading and are not considered here. Unlike the 2-DOS AGAs, Str interacts with the phosphate backbones of helices 44, 27 and 18 of 16S rRNA as well as the ribosomal protein S12; the latter is the hotspot for Str resistance mutations (PDB entry 8cgj)<sup>55</sup>. Ksg binds within the mRNA channel (PDB entry 8CEP)<sup>55</sup>. Spc binds to the end of helix 34 of 16S rRNA at the neck region of the SSU (PDB entry 8ca7)<sup>55</sup>. The nonaminoglycoside antibiotic tetracycline binds to the minor groove of helix 34 and the loop of helix 34 (PDB entry 8cf1)<sup>55</sup>.

**(c)** Apr (dark grey with DOS ring orange) primary binding site at the top of helix 44 (PDB entry 7PJS)<sup>54</sup>. DOS rings I and II are essential for the decoding site recognition and the stabilization of the error-prone conformation of the ribosome.

**(d)** Rank plot of genes with resistance mutations evolved in laboratory evolution experiments upon treatment with 2-DOS AGAs. Mutational analysis of 108 AGA-treated *Escherichia coli* strains were retrieved from the literature<sup>2,3,4,5,6,7,8,12,14,15,16</sup>. Categories of mutated genes are indicated. *fusA* is by far the most sampled gene in laboratory evolution experiments.



### Supplementary Figure 2. Potential models of *fusA*-mediated resistance mechanisms, related to Figure 1

Models 1 and 2 suggest that EF-G resistance variants could indirectly contribute to resistance by affecting translation velocity. While the effect of EF-G resistant variants on translation have not been tested so far, at least two different models of resistance can be envisioned:

**Model 1. Direct slowdown of self-promoted AGA uptake.** If AGA-induced misreading is unchanged, slower translation with mutant EF-G might lead to a slower accumulation of faulty proteins. As a result, quality control machinery and efflux pumps could better cope with proteotoxic stress, resulting in a slower AGA uptake<sup>56,57,58</sup> and allowing cells to grow at otherwise lethal concentrations.

**Model 2. Adaption to slower translation.** Slower translation might change the proteome composition. Such changes could directly contribute to the resistome, for example, in *Pseudomonas aeruginosa*, *fusA1* mutations were reported to lead to elevated levels of mexXY efflux pumps and Type III secretion system (T3SS)<sup>28</sup>. However, the AGA resistance correlates poorly with mexXY expression levels<sup>59</sup>. In *Salmonella enterica*, *fusA* mutations were associated with lower levels of HemA, the enzyme which catalyzes the first committed step in heme biosynthesis, resulting in lower levels of respiration<sup>60</sup>, which is often associated

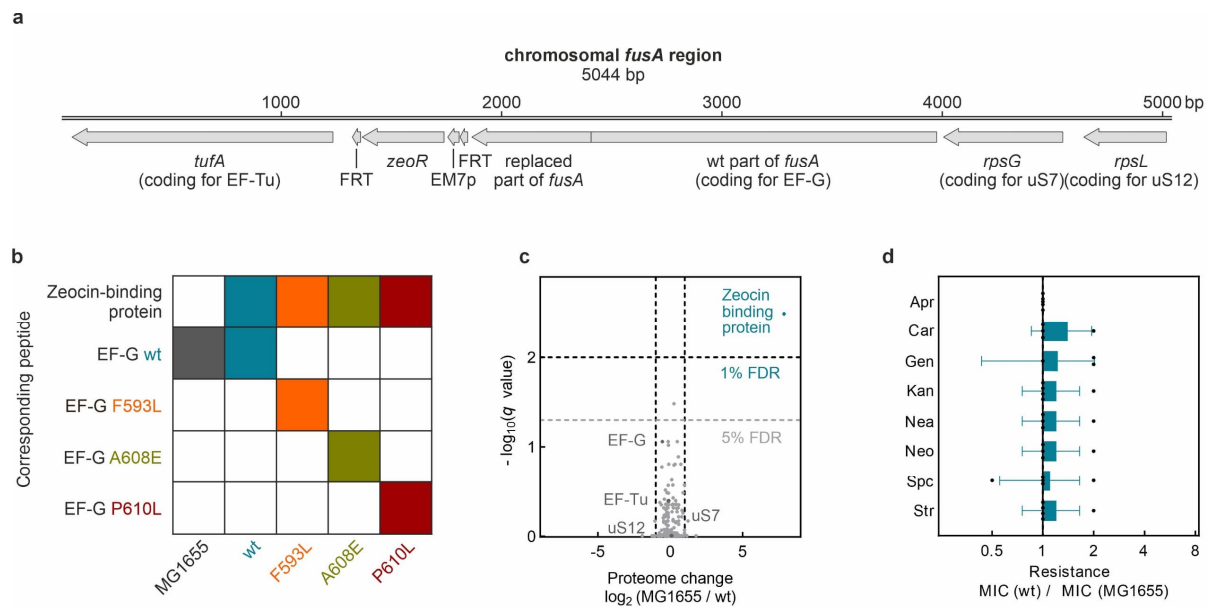
with higher AGA resistance. Alternatively, *fusA* mutations could indirectly render bacteria resistant by changes in the re-allocation of resources and metabolic fluxes, e.g., *fusA* mutations were proposed to disturb the levels of ppGpp<sup>61</sup>, a global transcription and translation regulator often associated with antibiotic resistance<sup>62</sup>.

Alternatively, models 3-5 suggest that EF-G resistance variants could directly interfere with AGA action on the ribosome:

Model 3. Allosteric displacement of the drug. None of the amino acid substitutions in EF-G are in close proximity to AGA on the ribosome, making the direct displacement of the drug unlikely. However, EF-G variants have been proposed to induce allosteric changes that lower the affinity of the drug to the ribosome<sup>8,24</sup>, similar to the mechanism of the tetracycline resistance protein Tet(O), an EF-G homolog, which uses its GTPase activity to remove tetracycline from the A site of the ribosome<sup>63</sup>.

Model 4. Gain of function. EF-G variants were suggested to facilitate translocation in the presence of AGA<sup>11</sup>, although such gain-of-function mechanism seems unlikely considering the widespread distribution of resistance mutations across EF-G.

Model 5. Ribosome silencing mechanism. EF-G variants could affect the error load in the AGA-affected cell. While EF-G variants do not restore the fidelity of AGA-bound ribosomes, because EF-G is not bound to the ribosome during decoding, they may affect formation of error clusters. If EF-G mutants slow down translation, AGA-bound ribosomes would perform fewer elongation cycles before the drug dissociates. Both the allosteric displacement (model 3) and the translation deceleration (model 5) could in principle alleviate error cluster formation and thus lower the proteotoxic burden that drives the self-promoted AGA uptake.



**Supplementary Figure 3. Generation and characterization of chromosomal *fusA* mutants, related to Figure 1**

**(a)** Schematic of the operon structure after insertion of *fusA* mutations. Correct insertion was confirmed by DNA sequencing.

**(b)** Targeted MS-based detection of EF-G variants. Each row corresponds to a particular peptide (Zeocin-binding protein, wt EF-G, or EF-G variant carrying one of the indicated mutations), while each column represents an *E. coli* strain (MG1655, wt, F593L, A608E, and P610L). A colored square indicates that the corresponding peptide was detected in that strain. Revertants or cross contaminations were not observed. The analysis confirms identity of the strains on the protein level.

**(c)** Proteome comparison of wt and MG1655 by quantitative MS (data independent acquisition). The volcano plot represents  $\log_2$ -fold changes in protein abundance (X-axis) and negative  $\log_{10}$  adjusted (Benjamini-Hochberg) *P* values (Y-axis) for the parental strain MG1655 to the wt strain ( $n=4$  biological replicates). Apart from the expression of the introduced zeocin resistance protein, the cloning strategy did not introduce significant proteomic changes. Notably, expression levels of EF-Tu, uS7 and uS12, which are members of the same operon, are not significantly altered.

**(d)** Comparison of the drug susceptibility of wt and MG1655. The minimal inhibitory concentrations (MIC) of all drugs tested are not significantly altered. Bars represent the mean  $\pm$  SD of 5 biological replicates ( $n=5$ ).



#### **Supplementary Figure 4. Proteome changes induced by *fusA* mutations, related to Figure 1**

**(a)** Subset of data from Figure 1D showing the regulation of proteins involved in AGA action or resistance. No systematic upregulation of porins or transporters that facilitate AGA entry into bacterial cell was observed<sup>64</sup>. Efflux pumps, including AcrA, AcrD, TolC (RND transporters), which promote AGA efflux in *E. coli*<sup>65,66</sup> were also not upregulated. Proteins involved in ppGpp-responsive regulation—which could potentially confer resistance via global reallocation of resources and major transcription factors orchestrating global stress responses—showed no significant changes. Similarly, chaperones and proteases linked to proteostasis<sup>67,68,69</sup> were not systematically upregulated. Finally, proteins previously identified in systematic screens as conferring AGA resistance upon overexpression<sup>70</sup> showed no consistent upregulation. These findings indicate that none of the known AGA resistance pathways are activated in *fusA* mutants.

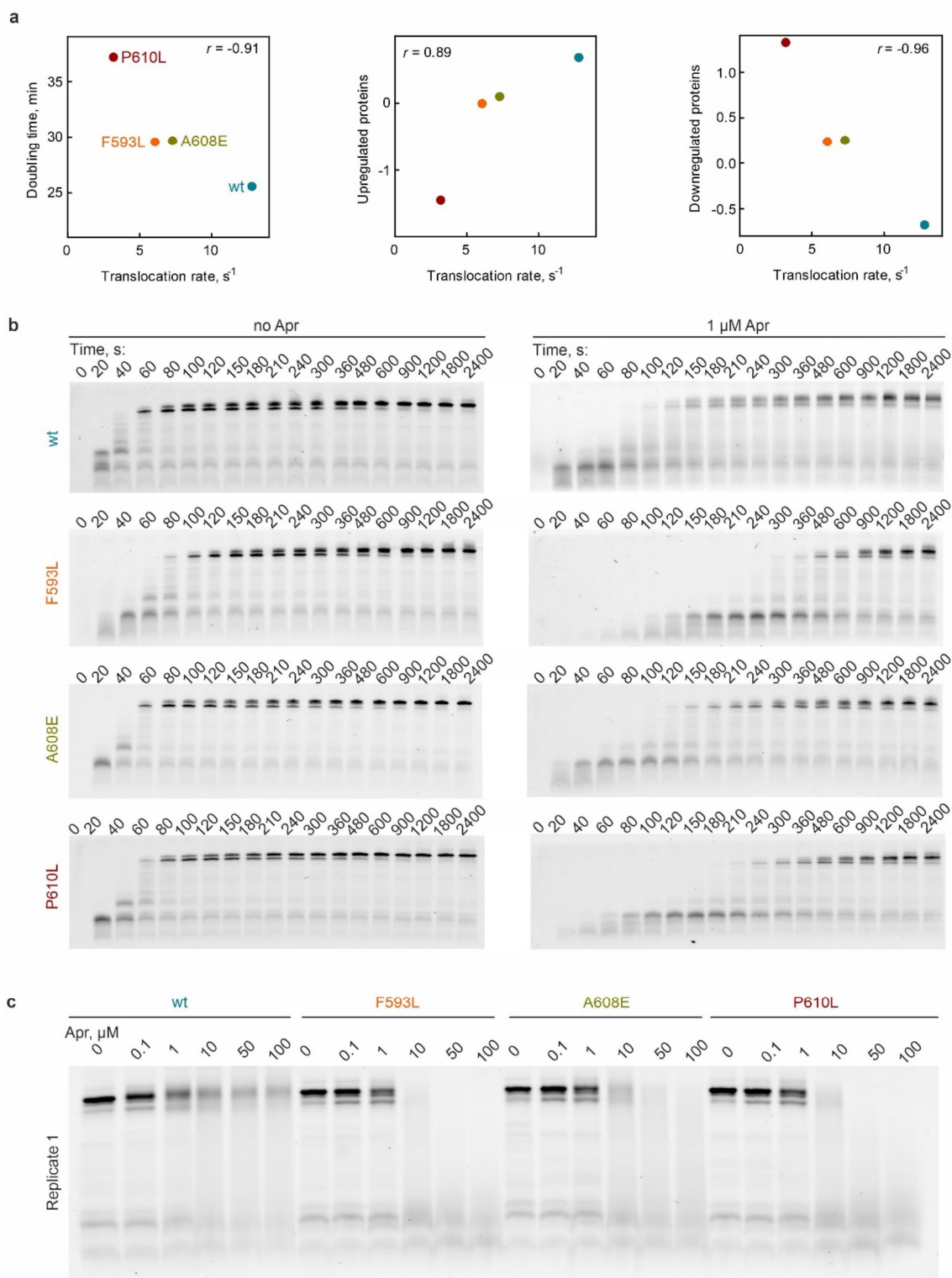
**(b)** Hierarchical clustering of significantly regulated proteins in MG1655, wt, and *fusA* mutants. Significantly regulated proteins were identified by multiple sample ANOVA test and compared by their Z-scores. Biological replicates (n = 4) were averaged. Proteins and strains were hierarchically clustered by their Euclidean distance and proteins were grouped in 5 clusters of co-regulated proteins. In the three minor clusters (saddle brown, dark orange, and magenta), proteins shared no common regulation pattern between *fusA* mutants and thus these proteins cannot constitute a common resistance mechanism. In contrast, in the two major clusters proteins were consistently down- (dark green, 234 proteins) or upregulated (blue, 163 proteins) in *fusA* mutant strains.

**(c)** Profile view of changes in expression levels of downregulated (upper panel) and upregulated (lower panel) proteins.

**(d)** Pearson correlation of cell growth and proteome adaptations. While overall the *fusA* mutants show only minor changes in their proteomes relative to the wt (Figure 1D), subtle adaptations of protein levels in the major clusters detected by hierarchical clustering correlate well with the growth rate differences (upper panel,  $P = 0.0002$ ; lower panel:  $P = 0.0039$ ).

**(e)** Correlation matrix of Pearson coefficients. Mutual correlation analysis of cell growth (Figure 1b), MIC values (Figure 1c), translocation rates (Figure 2a), and proteome regulation patterns (Figure S4b-d) across wt and *fusA* mutants (e.g. see Figures S4d, S5a). MIC values of different AGAs showed strong correlation, consistent with the idea that different *fusA* mutations confer resistance through a common mechanism. Cell growth, translocation rates, and proteome regulation patterns also correlate well, supporting the notion that proteome changes reflect subtle adaptations to the slower translocation rates and the resulting reduced growth. However, poor correlation between MICs values and growth-related metrics indicates that translocation rate differences, growth and proteome differences alone are not the primary drivers of AGA resistance.

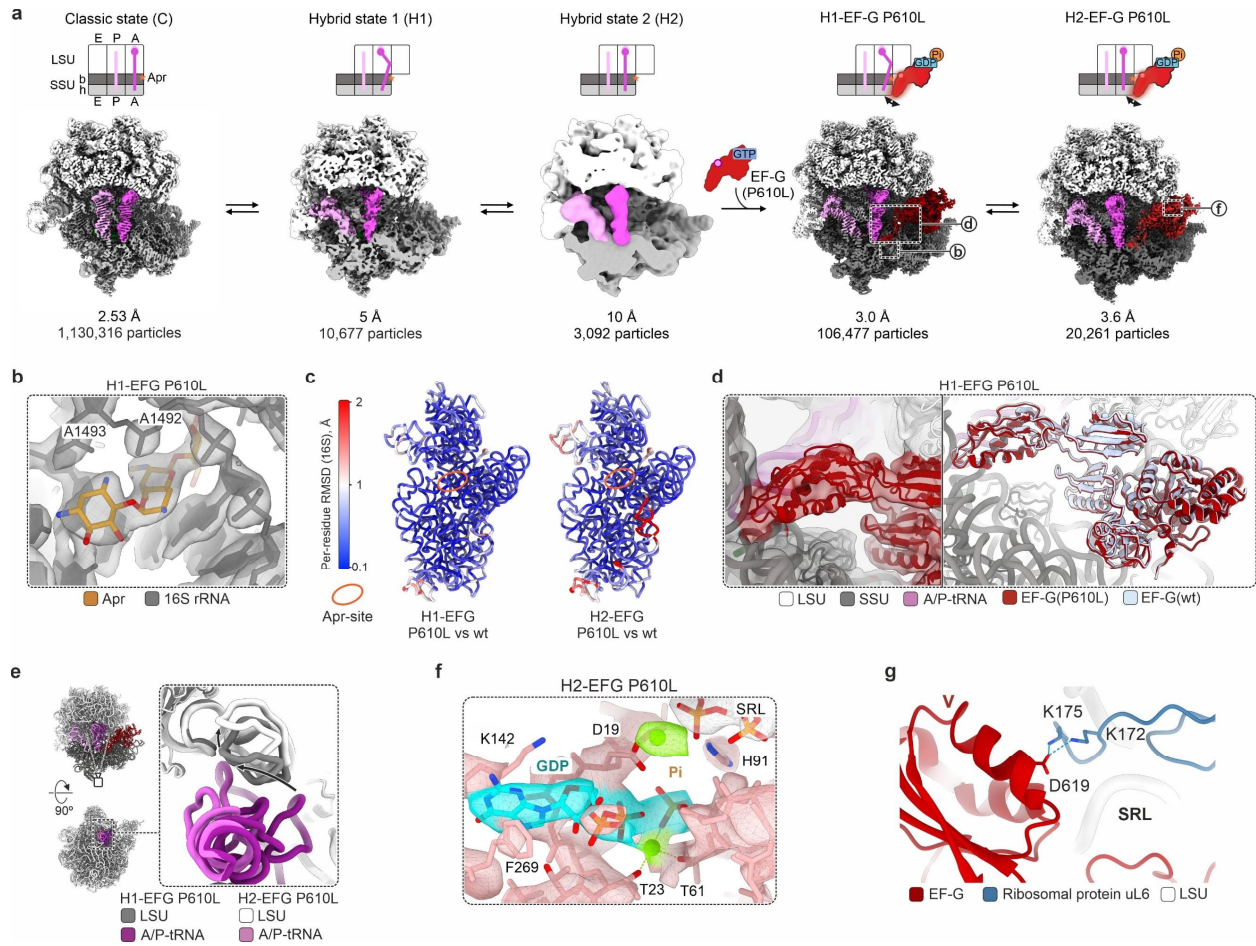
**(f)** Pathway enrichment analysis of protein clusters. Pathway enrichment analysis of the five protein clusters was performed using Fisher's exact test, with false discovery rate (FDR) correction by the Benjamini-Hochberg procedure. Members of only three pathways were significantly enriched in the clusters, all related to amino acid biosynthesis and upregulated in response to slower translation, which triggers translation attenuation mechanisms. These findings suggest that changes in translation rate drive misadaptive responses typically observed under starvation conditions, but do not explain the observed resistance pattern (Figure S4e).



**Supplementary Figure 5. Effect of EF-G variants and Apr on single-codon translocation and translation in vitro, related to Figure 2**

**(a)** Correlation of the translocation rates measured in single-codon assay with growth rates (left panel) and proteome changes (center and right panel) for wt EF-G (blue symbol), F593L (orange), A608E (olive), and P610L (red). Data replotted from Figures 1b, 2a and S4b-d. Pearson coefficients as indicated.

**(b)** Time courses of *slyD* in-vitro translation with EF-G variants in the absence and presence of Apr (1  $\mu$ M).  
**(c)** Dependence of SlyD formation on Apr concentration. Full length product was quantified after 30 min of translation in the absence and presence of increasing Apr concentrations.



**Supplementary Figure 6. Structural dynamics of EF-G P610L-driven translocation in presence of Apr, related to Figure 3**

**(a)** Cryo-EM analysis of EF-G P610L-promoted translocation in the presence of Apr. Top: Schematics of tRNA positions. The arrows indicate dynamics of the tip of EF-G domain IV, similar to that observed for EF-G wt<sup>54</sup>. Bottom: Cryo-EM maps with respective overall resolution in Å and number of cryo-EM particle images. In Figure 3a-d, hybrid state (H) refers to the major tRNA hybrid state H1, while in Figure 3e hybrid state (H) summarizes H1 and H2 particle populations.

**(b)** Apr bound in the decoding center of the ribosomal complex with EF-G P610L and GDP-Pi in state H1.

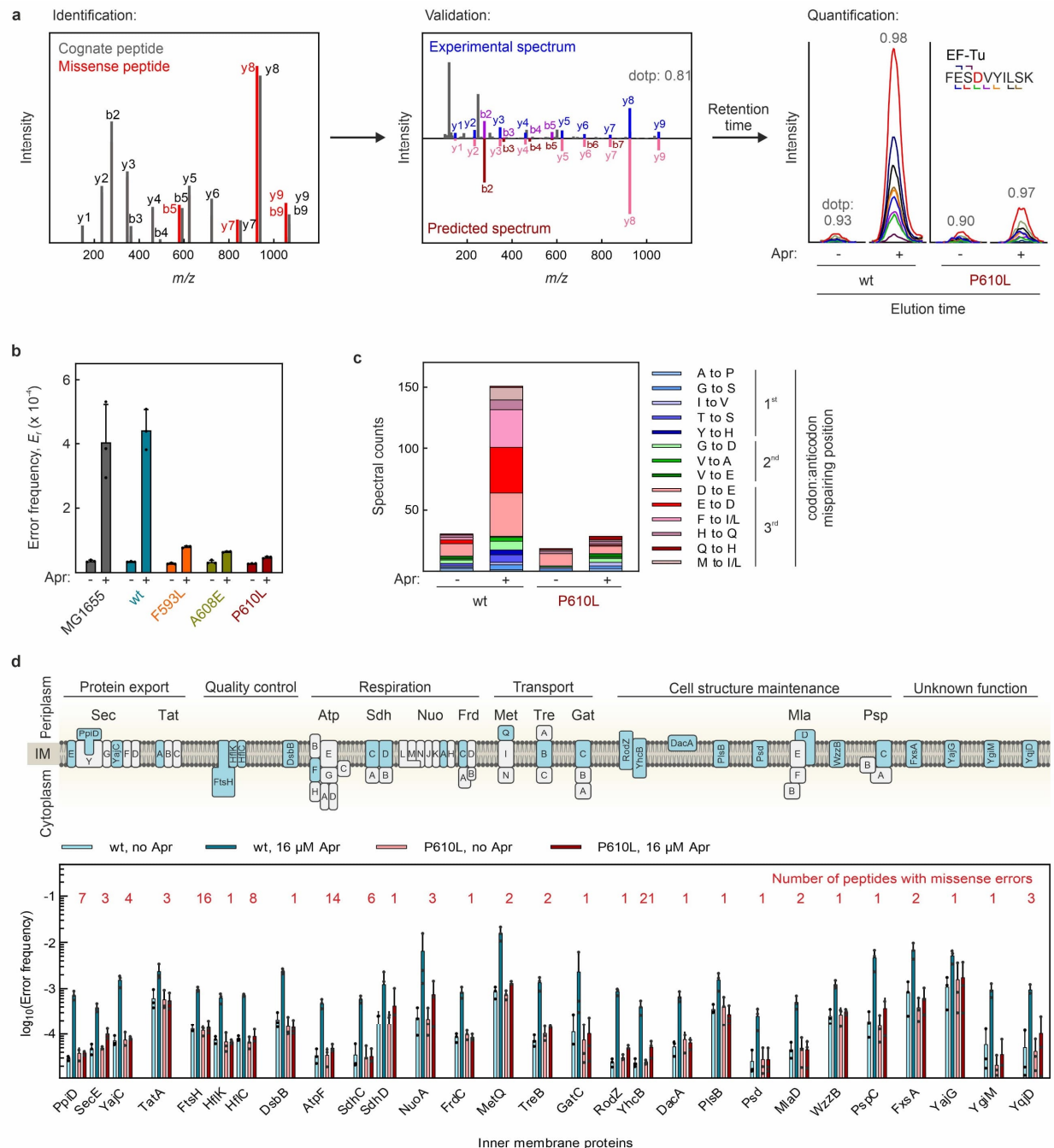
**(c)** Per-residue RMSDs of 16S rRNA between EF-G P610L- and wt-bound complexes, revealing generally negligible structural differences, particularly at the Apr-binding site (orange circle). H1-EF-G wt: PDB 7PJV; H2-EF-G wt: PDB 7PJW<sup>54</sup>.

**(d)** Structure of EF-G P610L-GDP-Pi in H1. Left: Cryo-EM density for domain IV, low-pass filtered to local resolution (6 Å). Right: Superposition with wt EF-G-GDP-Pi in H1 state (PDB 7PJW<sup>54</sup>), based on alignment by 23S rRNA.

**(e)** Repositioning of the elbow of A/P tRNA and helix 38 of 23S rRNA (H38) upon transition between tRNA hybrid states.

**(f)** Nucleotide binding pocket of EF-G P610L-GDP-Pi in H2.

**(g)** Interaction of LSU protein uL6 with domain V of EF-G. In the fusidic acid stalled ribosome-EF-G complex, residues K172 and K175 of uL6 form salt-bridges with D619 of EF-G (PDB 4V5F<sup>71</sup>); residues numbered according to *Thermus thermophilus* components here.



**Supplementary Figure 7. Preservation of proteome integrity in *fusA* mutant strains, related to Figure 4**

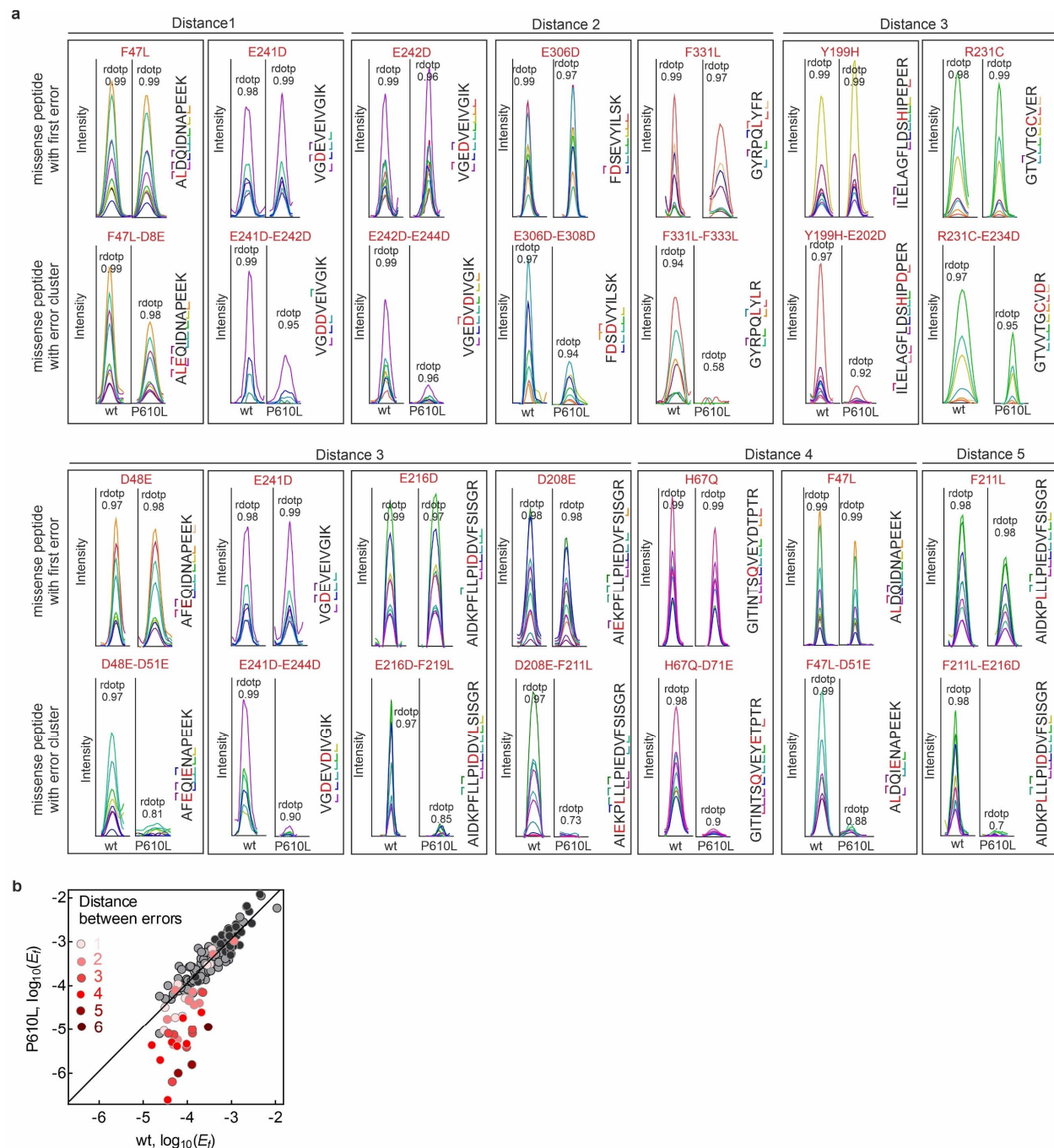
**(a)** Workflow for the identification, validation, and quantification of missense peptides with individual amino acid substitutions. Using the MaxQuant Dependent Peptide feature<sup>72</sup>, missense peptide candidates are identified by comparing MS/MS spectra of correct and missense peptides ensuring the confident localization of the amino acid substitution (shown is a peptide with the substitution E308D, corresponding to a -14 delta mass). Missense peptide candidates are validated by matching their MS/MS spectra with fragmentation spectra predicted *in-silico* by the deep neural network ProSIT<sup>73</sup>. Established fragmentation pattern and chromatographic retention times are used to quantify missense peptides across various biological states by label-free Parallel Reaction Monitoring (PRM). PRM traces are extracted

in Skyline <sup>74</sup>. Extracted fragment ions are color coded; amino acid substitutions indicated in red. Peptide abundances are calculated by integrating the signal of their co-eluting peptide fragments and error frequencies are estimated as the ratio of missense peptide and correct peptides abundances (see Methods).

**(b)** *fusA* mutations prevent Apr-induced (16  $\mu$ M) translational misreading. Bars represent the mean error frequencies  $\pm$  SD of 3 biological replicates (n=3) of the median of 28 misreading events.

**(c)** Semiquantitative analysis of the error burden in the proteome through spectral counting. Untreated and Apr-treated wt and P610L cells were lysed and proteins fractionated by SDS-PAGE. Missense peptide identifications in various proteins were counted (detection and identification as described above). Only types of substitutions whose counts are induced  $> 3$ -fold by AGA treatment were included. Position of the mismatch in the codon-anticodon interaction as indicated.

**(d)** Error frequencies in inner membrane proteins in the absence and presence of Apr (16  $\mu$ M, 60 min). Error frequencies of 109 misreading events in 28 proteins were determined by label free PRM. Bars represent mean error frequencies  $\pm$  SD of three biological replicates (n=3) of the medians of 1-21 misreading events per protein, as indicated above the bars.

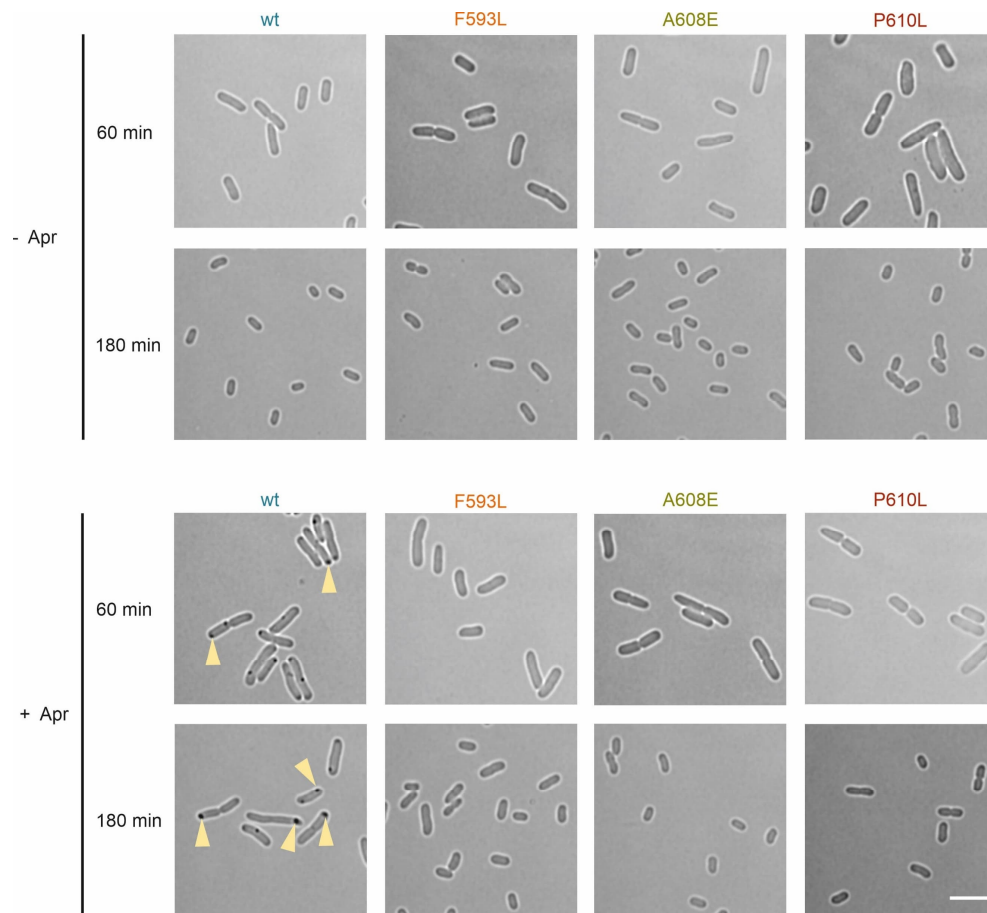


**Supplementary Figure 8. *fusA* mutations prevent error cluster formation, related to Figure 5**

**(a)** Chromatograms of eluting missense peptides with first errors and corresponding error clusters at induced conditions (wt: at 8-16  $\mu$ M Apr; P610L: at 128-256  $\mu$ M Apr; data are shown in Figure 5a,c). The conditions were chosen to ensure similar levels of single substituted peptides in wt and P610L. Extracted fragment ions are color-coded; amino acid substitutions indicated in red. Missense peptides were identified by the high sequence coverage, the coelution and identical fragmentation as of the spiked-in isotope-labeled reference peptides (ratio dot products  $\geq 0.97$ ). While missense peptides with short error clusters are often high abundant in wt and P610L cells, error clusters with more amino acid residues between the consecutive errors were strongly suppressed in P610L. To study this length effect in detail

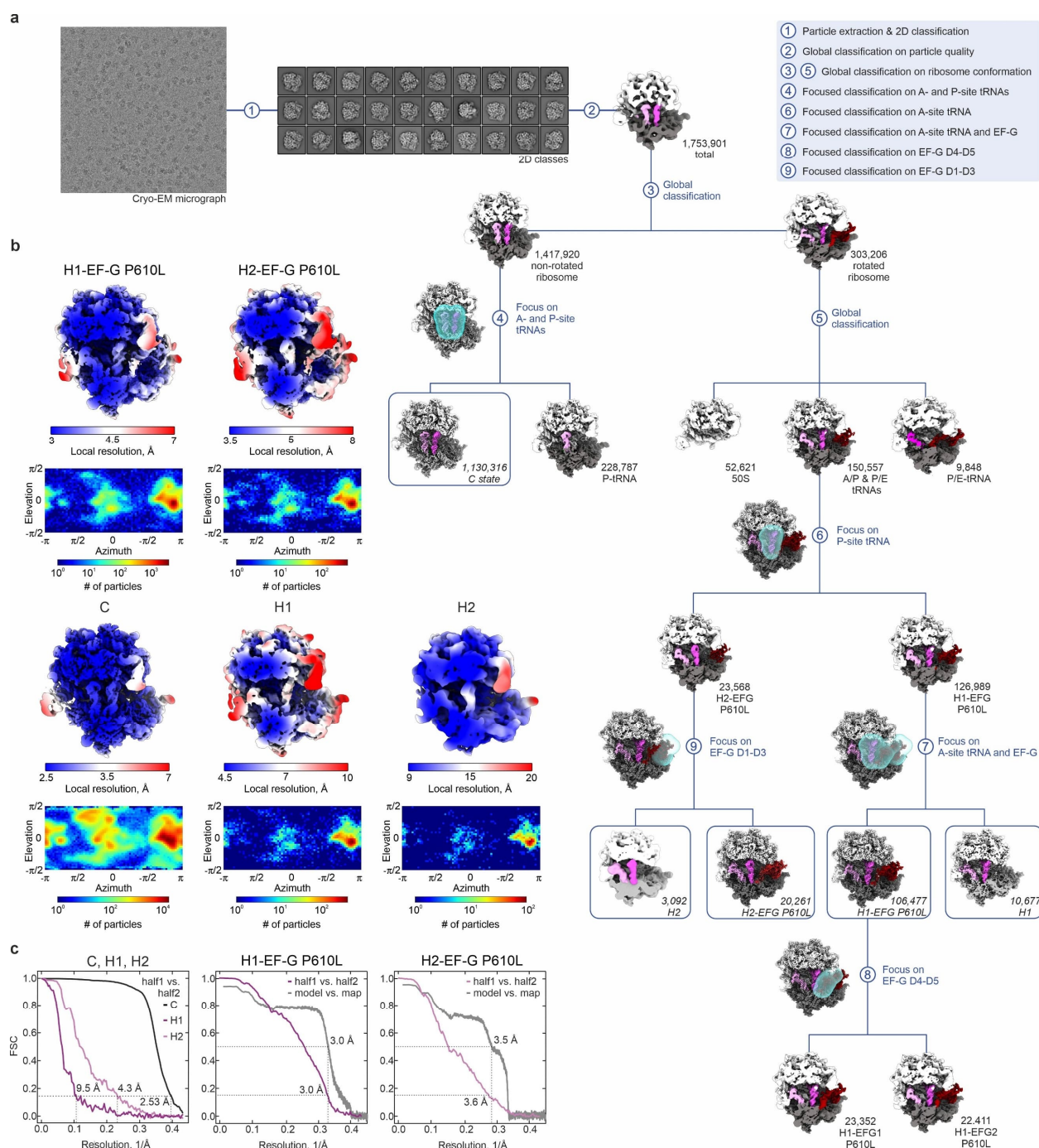
we extended set of error clusters from 14 to 38 in Figures 5d and S8b. Plots represent the MS2 intensities of peptide fragments (Y-axis) over the retention time (X-axis).

**(b)** Comparison of the error load with single errors and error clusters between wt and P610L at conditions of maximal misreading (wt at 16  $\mu$ M Apr, P610L at 256  $\mu$ M Apr). Missense peptides with error clusters are less abundant in P610L than in wt cells (red circles, quantified by PRM). This effect depends on the distance between the first and the consecutive amino acid substitution (see replot in Figure 5d). In contrast to error cluster formation, EF-G (P610L) had no significant effect on other misreading events: Grey circles, single errors quantified by MS1-filtering in DDA runs; black circles, single errors quantified by targeted MS (PRM). The type of data acquisition had no impact on this conclusion. This shows that *fusA* mutations prevent error cluster formation, but have otherwise no significant impact on the proteome integrity indicating that the intrinsic ribosome fidelity is unaltered, consistent with the fact that EF-G does not affect decoding per se. Because error frequencies are influenced by the concentrations of competing aminoacyl-tRNAs<sup>75</sup>, this also suggests that stoichiometries of cellular tRNAs are not substantially altered.



**Supplementary Figure 9. *FusA* mutations prevent protein aggregation in vivo, related to Figure 6**

Upper panel: brightfield images of wt and *fusA* mutant cells after 60 min and 180 min in the absence of Apr. Lower panel: same for cells after 60 min and 180 min of Apr treatment (16  $\mu$ M). Images for 180 min time point same as Figure 6a. Yellow arrows point to inclusion bodies. Scale bar, 5  $\mu$ m.



### Supplementary Figure 10. Cryo-EM analysis, related to Methods

**(a)** Multi-step sorting of cryo-EM data with exemplary micrograph 2D classes and 3D classes together with masks used for focused classification. See Methods for details.

**(b)** Local resolutions and angular distributions of final cryo-EM maps.

**(c)** Fourier-Shell-Correlation curves of final cryo-EM reconstructions, computed between half-maps (half1 vs. half2), and between full maps and atomic models (model vs. map), respectively. Atomic models were built for EF-G P610L-bound complexes only.

# Supplementary Figures

**Supplementary Table 1.** Cryo-EM structure determination

|   |   |   |
|---|---|---|
| <b>Ribosomal complex</b>                        | H1-EF-G P610L   | H2-EF-G(P610L)  |
| Ribosomal state                                 | tRNA hybrid state 1 with<br>EF-G P610L in GDP-Pi form | tRNA hybrid state 2 with<br>EF-G P610L in GDP-Pi form |
| <b>Database entries</b>                         |   |   |
| EMDB ID   | <b>EMD-54253</b>                                      | <b>EMD-54254</b>                                      |
| PDB ID  | <b>9RTU</b>   | <b>9RTV</b>   |
| <b>Data collection</b>                          |   |   |
| Microscope                                      | Titan Krios   | Titan Krios   |
| Camera  | Falcon III  | Falcon III  |
| Magnification                                   | 59,000  | 59,000  |
| Voltage (kV)                                    | 300   | 300   |
| Electron dose (e <sup>-</sup> /Å <sup>2</sup> ) | 30  | 30  |
| Defocus range (μm)                              | 0.2-1.5   | 0.2-1.5   |
| Pixel size (Å)                                  | 1.16  | 1.16  |
| <b>Cryo-EM reconstruction</b>                   |   |   |
| Final particles (no.)                           | 106,477   | 20,261  |
| Point group symmetry                            | <i>C1</i>   | <i>C1</i>   |
| FSC-threshold                                   | 0.143   | 0.143   |
| Resolution <sup>§</sup> (Å)                     | 3.0   | 3.6   |
| Resolution metric                               | gold standard FSC                                     | gold standard FSC                                     |
| <b>Atomic model refinement*</b>                 |   |   |
| Resolution <sup>§</sup> (Å)                     | 3.0   | 3.5   |
| Cumulative RSCC (%) >0.8/>0.6/>0.4              | 0.44/0.89/0.95  | 0.40/0.89/0.96  |
| Initial models used                             | PDB 7PJV  | PDB 7PJW  |
| Molprobity score                                | 1.64  | 1.74  |
| Clashscore                                      | 4.83  | 6.08  |
| <b>No. Atoms/No. Residues/RSCC</b>              |   |   |
| Total   | 0.75  | 0.74  |
| Protein   | 0.72  | 0.71  |
| Nucleic acids                                   | 0.78  | 0.77  |
| EF-G  | 0.63  | 0.60  |
| <b>B-factors</b>                                |   |   |
| Protein   | 37.60   | 47.56   |
| Nucleotide                                      | 31.92   | 54.35   |
| Ligands, Ions                                   | 18.84   | 34.55   |
| <b>R.m.s. deviations</b>                        |   |   |
| Bond lengths (Å)                                | 0.005   | 0.005   |
| Bond angles (°)                                 | 0.644   | 0.978   |
| <b>Ramachandran plot</b>                        |   |   |
| Favored (%)                                     | 94.21   | 93.89   |
| Allowed (%)                                     | 5.79  | 6.09  |
| Disallowed (%)                                  | 0.00  | 0.02  |

<sup>§</sup>Resolution used for atomic model refinement and interpretation.

\*For model refinement, the high-resolution H1-EF-G P610L map was resampled to 512×512×512 pixels, corresponding to a pixel size of 0.6525Å

<sup>§</sup>Resolution at which map-model FSC=0.5.

**Supplementary Table 2. Resources**

| REAGENT or RESOURCE  | SOURCE                              | IDENTIFIER       |
|--|-------------------------------------|------------------|
| <b>Strains</b>   |                                     |                  |
| MG1655   | Leibniz Institute DSMZ              | DSM 18039        |
| BL21(DE3)  | Thermo Fisher Scientific            | EC0114           |
| Engineered <i>fusA</i> strains<br>(parental strain MG1655)                 | Genetic engineering<br>Heidelberg   | This manuscript  |
| <b>Plasmids &amp; Recombinant DNA</b>                                      |                                     |                  |
| pET-24a vector, Kan resistance   | Novagen                             |                  |
| pRed/ET  | Genetic Engineering<br>Heidelberg   |                  |
| pET-24a ( <i>fusA</i> _wt), <i>fusA</i><br>sequence derived from<br>MG1655 |                                     | This manuscript  |
| pET-24a ( <i>fusA</i> _G117C)  | based on pET-24a ( <i>fusA</i> _wt) | This manuscript  |
| pET-24a ( <i>fusA</i> _R371L)  | based on pET-24a ( <i>fusA</i> _wt) | This manuscript  |
| pET-24a ( <i>fusA</i> _F593C)  | based on pET-24a ( <i>fusA</i> _wt) | This manuscript  |
| pET-24a ( <i>fusA</i> _F593L)  | based on pET-24a ( <i>fusA</i> _wt) | This manuscript  |
| pET-24a ( <i>fusA</i> _F605I)  | based on pET-24a ( <i>fusA</i> _wt) | This manuscript  |
| pET-24a ( <i>fusA</i> _A608E)  | based on pET-24a ( <i>fusA</i> _wt) | This manuscript  |
| pET-24a ( <i>fusA</i> _A608V)  | based on pET-24a ( <i>fusA</i> _wt) | This manuscript  |
| pET-24a ( <i>fusA</i> _P610L)  | based on pET-24a ( <i>fusA</i> _wt) | This manuscript  |
| pET-24a ( <i>fusA</i> _P610Q)  | based on pET-24a ( <i>fusA</i> _wt) | This manuscript  |
| pET-24a ( <i>fusA</i> _T674A)  | based on pET-24a ( <i>fusA</i> _wt) | This manuscript  |
| pET-24a ( <i>fusA</i> _A678V)  | based on pET-24a ( <i>fusA</i> _wt) | This manuscript  |
| pET-24a ( <i>fusA</i> _Y680C)  | based on pET-24a ( <i>fusA</i> _wt) | This manuscript  |
| <b>Oligonucleotides</b>  |                                     |                  |
| MF+14Flu mRNA  | IBA lifesciences                    |                  |
| <b>Chemicals, peptides,<br/>recombinant proteins</b>                       |                                     |                  |
| cOmplete protease inhibitor  | Roche                               | Cat# 11697498001 |
| DNase I  | Thermo Fisher Scientific            | Cat# EN0521      |
| Apramycin (Apr)  | Sigma-Aldrich                       | Cat# A2024       |
| Carbenecillin (Car)  | Carl Roth                           | Cat# 6344.3      |
| Chloramphenicol (Cam)  | Sigma-Aldrich                       | Cat# C1919       |
| Dihydrostreptomycin (Dhs)  | Sigma-Aldrich                       | Cat# D7253       |
| Erythromycin (Ery)   | Sigma-Aldrich                       | Cat# 856193      |
| Gentamicin (Gen)   | Sigma-Aldrich                       | Cat# G1264       |
| KanamycinA (KanA)  | Sigma-Aldrich                       | Cat# K4000       |
| Kanamycin B (KanB)   | Sigma-Aldrich                       | Cat# B5264       |
| Kasugamycin (Ksg)  | Sigma-Aldrich                       | Cat# 32354       |
| Neamine (Nea)  | Santa Cruz Biotechnology            | Cat# sc-338357   |
| NeomycinB (Neo)  | Sigma-Aldrich                       | Cat# N6386       |
| Norfloxacin (Nor)  | Sigma-Aldrich                       | Cat# N9890       |
| Ribostamycin (Rib)   | Sigma-Aldrich                       | Cat# R2255       |
| Sisomicin (Sis)  | Sigma-Aldrich                       | Cat# S7796       |

|   |   |   |
|---|---|---|
| Spectinomycin (Spc)                                     | TCI   | Cat# SO584  |
| Streptomycin (Str)                                      | Sigma-Aldrich                               | Cat# S9137  |
| Tetracycline (Tet)                                      | Sigma-Aldrich                               | Cat# T7660  |
| DTT (Cleland's reagent, ULTROL)                         | Merck                                       | Cat# 233153   |
| Iodoacetamide   | Sigma-Aldrich                               | Cat# I1149  |
| Bodipy-FL-succinimidyl ester                            | Thermo Fisher Scientific                    | Cat# D6102  |
| Gentamicin Texas Red (GTTR)                             | AAT Bioquest                                | Cat# 24300  |
| Isotope-labeled reference peptides                      | JPT Peptide Technologies                    | Spike-Tides L   |
| Trypsin (Sequencing Grade modified)                     | Promega                                     | Cat# V5111  |
| <b>Critical commercial assays</b>                       |   |   |
| LIVE/DEAD® BacLight™ Bacterial Viability Kit            | Invitrogen                                  | Cat# L7012  |
| Protino Ni-IDA 2000                                     | Macherey-Nagel                              | Cat# 745170.25  |
| <b>Software and algorithms</b>                          |   |   |
| MaxQuant 2.0.1.0 & 2.1.4.0                              | Cox and Mann (2008) <sup>76</sup>           | 10.1038/nbt.1511  |
| Perseus 1.6.15.0  | Tyanova, Temu, and Cox (2016) <sup>77</sup> | <a href="https://maxquant.net/perseus/">https://maxquant.net/perseus/</a>   |
| PEAKS 10.5  | Bioinformatics Solutions Inc.               | <a href="https://www.bioinfor.com/">https://www.bioinfor.com/</a>   |
| Skyline 24.1.0.199                                      | Pino et al. (2020) <sup>78</sup>            | 10.1002/mas.21540   |
| Spectronaut 17.1.22                                     | Biognosys                                   | <a href="https://biognosys.com">https://biognosys.com</a>   |
| Algorithm for the detection of amino acid substitutions | Mordret et al. (2019) <sup>79</sup>         | 10.1016/j.molcel.2019.06.041  |
| GraphPad PRISM 10                                       | GraphPad Software, Boston                   | <a href="http://www.graphpad.com">www.graphpad.com</a>  |
| Multi Gauge   | FUJIFILM                                    | N/A   |
| MicrobeJ 5.14   | Ducret et al. (2016) <sup>80</sup>          | <a href="https://www.microbej.com/">https://www.microbej.com/</a>   |
| Fiji 2.14   | NIH, Bethesda <sup>81</sup>                 | <a href="https://imagej.nih.gov/ij/">https://imagej.nih.gov/ij/</a>   |
| Zen Black 2.3   | Zeiss                                       | <a href="https://www.zeiss.com/microscopy/us/products/software/zeiss-zen.html">https://www.zeiss.com/microscopy/us/products/software/zeiss-zen.html</a> |
| BioRender   | BioRender                                   | <a href="https://BioRender.com/40melak">https://BioRender.com/40melak</a>   |
| CorelDRAW 26.1.0.143                                    | Corel Corporation                           | <a href="https://www.coreldraw.com/de/">https://www.coreldraw.com/de/</a>   |
| CETCORPLUS 4.6.9  | CEOS Heidelberg                             | <a href="https://www.ceos-gmbh.de/de">https://www.ceos-gmbh.de/de</a>   |
| ChimeraX 1.8-1.10.1                                     | Pettersen et al. (2021) <sup>82</sup>       | <a href="https://www.rbvi.ucsf.edu/chimera">https://www.rbvi.ucsf.edu/chimera</a>   |
| WinCoot 0.9.8.95  | Brown et al. (2015) <sup>83</sup>           | <a href="https://www2.mrc-lmb.cam.ac.uk/personal/pemsl ey/coot">https://www2.mrc-lmb.cam.ac.uk/personal/pemsl ey/coot</a>                               |
| CTFFIND-4.1   | Rohou and Grigorieff (2015) <sup>84</sup>   | <a href="https://grigoriefflab.umassmed.edu/ctffind4">https://grigoriefflab.umassmed.edu/ctffind4</a>   |
| EPU 2.3   | Thermo Fisher Eindhoven                     | <a href="https://www.thermofisher.com/de/de/home/electron-">https://www.thermofisher.com/de/de/home/electron-</a>                                       |

|                                  |  |   |
|----------------------------------|--|---|
|                                  |  | microscopy/products/software-em-3d-vis/software-updates.html  |
| Gautomatch 0.56                  | Dr. Kai Zhang                                      | <a href="https://www.mrc-lmb.cam.ac.uk/kzhang">https://www.mrc-lmb.cam.ac.uk/kzhang</a>   |
| MotionCor2                       | Zheng et al. (2017) <sup>85</sup>                  | <a href="https://emcore.ucsf.edu/ucsf-software">https://emcore.ucsf.edu/ucsf-software</a>   |
| PHENIX 1.20.1                    | Liebschner et al. (2019) <sup>86</sup>             | <a href="https://www.phenix-online.org">https://www.phenix-online.org</a>   |
| RELION 3.1 & 5.0                 | Zivanov et al. (2018) <sup>87</sup>                | <a href="https://www3.mrc-lmb.cam.ac.uk/relion">https://www3.mrc-lmb.cam.ac.uk/relion</a>   |
| Xcalibur™ 4.3                    | Thermo Fisher                                      |   |
| <b>Other</b>                     |  |   |
| Starion IR/FLA-9000 scanner      | FUJIFILM   |   |
| FERAstar FS platereader          | BMG Labtech  |   |
| Orbitrap Exploris 480            | Thermo Fisher                                      |   |
| Orbitrap Fusion Lumos Tribrid    | Thermo Fisher                                      |   |
| Centrifuges                      | Beckman Avanti J-30I, JA 25.50 rotor               |   |
| Ultracentrifuges                 | Beckman Optima L-100XP, Ti 50.2 rotor & SW32 rotor |   |
| EmulsiFlex C3                    | AVESTIN  |   |
| LSM880                           | Zeiss  | <a href="https://www.zeiss.com/microscopy/us/products/light-microscopes/confocal-microscopes/airyscan.html">https://www.zeiss.com/microscopy/us/products/light-microscopes/confocal-microscopes/airyscan.html</a> |
| Stopped flow apparatus           | Applied Photophysics                               |   |
| <b>Deposited structural data</b> |  |   |
| Structure of C state             | Petrychenko et. al. (2021) <sup>54</sup>           | PDB: 7PJV   |
| Structure of H1-EFG wt           | Petrychenko et. al. (2021) <sup>54</sup>           | PDB: 7PJV   |
| Structure of H2-EFG wt           | Petrychenko et. al. (2021) <sup>54</sup>           | PDB: 7PJW   |
| Structure of C state             | This study   | EMDB: 55123   |
| Structure of H1 state            | This study   | EMDB: 55124   |
| Structure of H2 state            | This study   | EMDB: 55125   |
| Structure of H1-EF-G P610L       | This study   | PDB: 9RTU; EMDB: 54253  |
| Structure of H2-EF-G P610L       | This study   | PDB: 9RTV; EMDB: 54254  |

## Supplementary References

1. Wohlgenuth I., *et al.* Translation error clusters induced by aminoglycoside antibiotics. *Nat. Commun.* **12**, 1830 (2021).
2. Sulaiman J. E., Lam H. Proteomic investigation of tolerant *Escherichia coli* populations from cyclic antibiotic treatment. *J. Proteome. Res.* **19**, 900-913 (2020).
3. Porse A., Jahn L. J., Ellabaan M. M. H., Sommer M. O. A. Dominant resistance and negative epistasis can limit the co-selection of de novo resistance mutations and antibiotic resistance genes. *Nat. Commun.* **11**, 1199 (2020).
4. Hoeksema M., Jonker M. J., Brul S., Ter Kuile B. H. Effects of a previously selected antibiotic resistance on mutations acquired during development of a second resistance in *Escherichia coli*. *BMC Genomics* **20**, 284 (2019).
5. Lázár V., *et al.* Bacterial evolution of antibiotic hypersensitivity. *Mol. Syst. Biol.* **9**, 700 (2013).
6. Ghaddar N., Hashemidahaj M., Findlay B. L. Access to high-impact mutations constrains the evolution of antibiotic resistance in soft agar. *Sci. Rep.* **8**, 17023 (2018).
7. Jahn L. J., Munck C., Ellabaan M. M. H., Sommer M. O. A. Adaptive laboratory evolution of antibiotic resistance using different selection regimes lead to similar phenotypes and genotypes. *Front. Microbiol.* **8**, 816 (2017).
8. Ibacache-Quiroga C., Oliveros J. C., Couce A., Blázquez J. Parallel evolution of high-level aminoglycoside resistance in *Escherichia coli* under low and high mutation supply rates. *Front. Microbiol.* **9**, 427 (2018).
9. Hickman R. A., Munck C., Sommer M. O. A. Time-resolved tracking of mutations reveals diverse allele dynamics during *Escherichia coli* antimicrobial adaptive evolution to single drugs and drug pairs. *Front Microbiol* **8**, 893 (2017).
10. Hou Y., Lin Y. P., Sharer J. D., March P. E. *In vivo* selection of conditional-lethal mutations in the gene encoding elongation factor G of *Escherichia coli*. *J. Bacteriol.* **176**, 123-129 (1994).
11. Mogre A., Sengupta T., Veetil R. T., Ravi P., Seshasayee A. S. Genomic analysis reveals distinct concentration-dependent evolutionary trajectories for antibiotic resistance in *Escherichia coli*. *DNA Res.* **21**, 711-726 (2014).
12. Oz T., *et al.* Strength of selection pressure is an important parameter contributing to the complexity of antibiotic resistance evolution. *Mol. Biol. Evol.* **31**, 2387-2401 (2014).
13. Usui M., Yoshii Y., Thiriet-Rupert S., Ghigo J. M., Beloin C. Intermittent antibiotic treatment of bacterial biofilms favors the rapid evolution of resistance. *Commun. Biol.* **6**, 275 (2023).
14. Qi W., Jonker M. J., de Leeuw W., Brul S., Ter Kuile B. H. Reactive oxygen species accelerate de novo acquisition of antibiotic resistance in *E. coli*. *iScience* **26**, 108373 (2023).
15. Callens M., *et al.* Hypermutator emergence in experimental *Escherichia coli* populations is stress-type dependent. *Evol. Lett.* **7**, 252-261 (2023).
16. Qi W., Jonker M. J., de Leeuw W., Brul S., Ter Kuile B. H. Role of RelA-synthesized (p)ppGpp and ROS-induced mutagenesis in de novo acquisition of antibiotic resistance in *E. coli*. *iScience* **27**, 109579 (2024).
17. Li X., *et al.* Nonsteroidal anti-inflammatory drug diclofenac accelerates the emergence of antibiotic resistance via mutagenesis. *Environ Pollut* **326**, 121457 (2023).
18. Daruka L., *et al.* ESKAPE pathogens rapidly develop resistance against antibiotics in development in vitro. *Nat. Microbiol.*, (2025).
19. Hernando-Amado S., Sanz-Garcia F., Martinez J. L. Antibiotic Resistance Evolution Is Contingent on the Quorum-Sensing Response in *Pseudomonas aeruginosa*. *Mol Biol Evol* **36**, 2238-2251 (2019).

20. Scribner M. R., Santos-Lopez A., Marshall C. W., Deitrick C., Cooper V. S. Parallel evolution of tobramycin resistance across species and environments. *mBio* **11**, (2020).
21. Santi I., Manfredi P., Maffei E., Egli A., Jenal U. Evolution of Antibiotic Tolerance Shapes Resistance Development in Chronic *Pseudomonas aeruginosa* Infections. *mBio* **12**, (2021).
22. Feng Y., Jonker M. J., Moustakas I., Brul S., Ter Kuile B. H. Dynamics of Mutations during Development of Resistance by *Pseudomonas aeruginosa* against Five Antibiotics. *Antimicrob Agents Chemother* **60**, 4229-4236 (2016).
23. Sanz-García F., Hernando-Amado S., Martínez J. L. Mutational evolution of *Pseudomonas aeruginosa* resistance to ribosome-targeting antibiotics. *Front. Genet.* **9**, 451 (2018).
24. Bolard A., Plésiat P., Jeannot K. Mutations in gene *fusA1* as a novel mechanism of aminoglycoside resistance in clinical strains of *Pseudomonas aeruginosa*. *Antimicrob. Agents Chemother.* **62**, (2018).
25. Rodriguez de Evgrafov M. C., Faza M., Asimakopoulos K., Sommer M. O. A. Systematic investigation of resistance evolution to common antibiotics reveals conserved collateral responses across common human pathogens. *Antimicrob. Agents Chemother.* **65**, (2020).
26. Ramsay K. A., McTavish S. M., Wardell S. J. T., Lamont I. L. The Effects of Sub-inhibitory Antibiotic Concentrations on *Pseudomonas aeruginosa*: Reduced Susceptibility Due to Mutations. *Front Microbiol* **12**, 789550 (2021).
27. Laborda P., Martínez J. L., Hernando-Amado S. Convergent phenotypic evolution towards fosfomycin collateral sensitivity of *Pseudomonas aeruginosa* antibiotic-resistant mutants. *Microb. Biotechnol.* **15**, 613-629 (2022).
28. Maunders E. A., Triniman R. C., Western J., Rahman T., Welch M. Global reprogramming of virulence and antibiotic resistance in *Pseudomonas aeruginosa* by a single nucleotide polymorphism in elongation factor, *fusA1*. *J. Biol. Chem.* **295**, 16411-16426 (2020).
29. Abisado-Duque R. G., *et al.* An Amino Acid Substitution in Elongation Factor EF-G1A Alters the Antibiotic Susceptibility of *Pseudomonas aeruginosa* LasR-Null Mutants. *J Bacteriol* **205**, e0011423 (2023).
30. Abisado R. G., *et al.* Tobramycin Adaptation Enhances Policing of Social Cheaters in *Pseudomonas aeruginosa*. *Appl Environ Microbiol* **87**, e0002921 (2021).
31. Wardell S. J. T., Rehman A., Martin L. W., Winstanley C., Patrick W. M., Lamont I. L. A large-scale whole-genome comparison shows that experimental evolution in response to antibiotics predicts changes in naturally evolved clinical *Pseudomonas aeruginosa*. *Antimicrob Agents Chemother* **63**, (2019).
32. Thacharodi A., Lamont I. L. Gene-gene interactions reduce aminoglycoside susceptibility of *Pseudomonas aeruginosa* through efflux pump-dependent and -independent mechanisms. *Antibiotics (Basel)* **12**, (2023).
33. Vestergaard M., Paulander W., Leng B., Nielsen J. B., Westh H. T., Ingmer H. Novel Pathways for Ameliorating the Fitness Cost of Gentamicin Resistant Small Colony Variants. *Front Microbiol* **7**, 1866 (2016).
34. Cao S., Huseby D. L., Brandis G., Hughes D. Alternative Evolutionary Pathways for Drug-Resistant Small Colony Variant Mutants in *Staphylococcus aureus*. *mBio* **8**, (2017).
35. Heidarian S., Guliaev A., Nicoloff H., Hjort K., Andersson D. I. High prevalence of heteroresistance in *Staphylococcus aureus* is caused by a multitude of mutations in core genes. *PLoS Biol* **22**, e3002457 (2024).
36. Ma S., *et al.* Mechanisms of *Staphylococcus aureus* Antibiotics Resistance Revealed by Adaptive Laboratory Evolution. *Curr Microbiol* **82**, 46 (2025).

37. Lozano-Huntelman N. A., *et al.* Evolution of antibiotic cross-resistance and collateral sensitivity in *Staphylococcus epidermidis* using the mutant prevention concentration and the mutant selection window. *Evol. Appl.* **13**, 808-823 (2020).
38. Boyd S. M., *et al.* Genomic characterization of antibiotic-resistant *Staphylococcus epidermidis* with observed shifts in optimal temperature. *J Appl Microbiol* **135**, (2024).
39. Holley C. L., *et al.* A single amino acid substitution in elongation factor G can confer low-level gentamicin resistance in *Neisseria gonorrhoeae*. *Antimicrob. Agents Chemother.* **66**, e0025122 (2022).
40. Golparian D., Jacobsson S., Holley C. L., Shafer W. M., Unemo M. High-level in vitro resistance to gentamicin acquired in a stepwise manner in *Neisseria gonorrhoeae*. *J Antimicrob Chemother* **78**, 1769-1778 (2023).
41. Waller N. J. E., Cheung C. Y., Cook G. M., McNeil M. B. The evolution of antibiotic resistance is associated with collateral drug phenotypes in *Mycobacterium tuberculosis*. *Nat. Commun.* **14**, 1517 (2023).
42. Kuhberger R., Piepersberg W., Petzet A., Buckel P., Bock A. Alteration of ribosomal protein L6 in gentamicin-resistant strains of *Escherichia coli*. Effects on fidelity of protein synthesis. *Biochemistry* **18**, 187-193 (1979).
43. Wasserman M. R., *et al.* Chemically related 4,5-linked aminoglycoside antibiotics drive subunit rotation in opposite directions. *Nat. Commun.* **6**, 7896 (2015).
44. Hobbie S. N., *et al.* Binding of neomycin-class aminoglycoside antibiotics to mutant ribosomes with alterations in the A site of 16S rRNA. *Antimicrob. Agents Chemother.* **50**, 1489-1496 (2006).
45. Bollen A., Cabezón T., de Wilde M., Villarroel R., Herzog A. Alteration of ribosomal protein S17 by mutation linked to neamine resistance in *Escherichia coli*. I. General properties of neaA mutants. *J Mol Biol* **99**, 795-806 (1975).
46. Yaguchi M., *et al.* Alteration of ribosomal protein S17 by mutation linked to neamine resistance in *Escherichia coli*. II. Localization of the amino acid replacement in protein S17 from a meaA mutant. *J Mol Biol* **104**, 617-620 (1976).
47. Yaguchi M., *et al.* Cooperative control of translational fidelity by ribosomal proteins in *Escherichia coli*. II. Localization of amino acid replacements in proteins S5 and S12 altered in double mutants resistant to neamine. *Mol Gen Genet* **142**, 35-43 (1975).
48. Peske F., Savelsbergh A., Katunin V. I., Rodnina M. V., Wintermeyer W. Conformational changes of the small ribosomal subunit during elongation factor G-dependent tRNA-mRNA translocation. *J. Mol. Biol.* **343**, 1183-1194 (2004).
49. Safdari H. A., *et al.* The translation inhibitors kasugamycin, edeine and GE81112 target distinct steps during 30S initiation complex formation. *Nat Commun* **16**, 2470 (2025).
50. Zhang Y., *et al.* The context of the ribosome binding site in mRNAs defines specificity of action of kasugamycin, an inhibitor of translation initiation. *Proc. Natl. Acad. Sci. USA.* **119**, (2022).
51. Bilgin N., Richter A. A., Ehrenberg M., Dahlberg A. E., Kurland C. G. Ribosomal RNA and protein mutants resistant to spectinomycin. *EMBO J* **9**, 735-739 (1990).
52. Kamath D., Gregory S. T., O'Connor M. The Loop 2 Region of Ribosomal Protein uS5 Influences Spectinomycin Sensitivity, Translational Fidelity, and Ribosome Biogenesis. *Antimicrob Agents Chemother* **61**, (2017).
53. Shapovalova K. S., *et al.* Synthesis and antibacterial activity of new 6"-modified tobramycin derivatives. *Antibiotics (Basel)* **13**, (2024).
54. Petrychenko V., Peng B. Z., de A. P. Schwarzer A. C., Peske F., Rodnina M. V., Fischer N. Structural mechanism of GTPase-powered ribosome-tRNA movement. *Nat. Commun.* **12**, 5933 (2021).
55. Paternoga H., *et al.* Structural conservation of antibiotic interaction with ribosomes. *Nat Struct Mol Biol* **30**, 1380-1392 (2023).

56. Taber H. W., Mueller J. P., Miller P. F., Arrow A. S. Bacterial uptake of aminoglycoside antibiotics. *Microbiol. Rev.* **51**, 439-457 (1987).
57. Davis B. D. Mechanism of bactericidal action of aminoglycosides. *Microbiol. Rev.* **51**, 341-350 (1987).
58. Baquero F., Levin B. R. Proximate and ultimate causes of the bactericidal action of antibiotics. *Nat Rev Microbiol* **19**, 123-132 (2021).
59. Seupt A., Schniederjans M., Tomasch J., Häussler S. Expression of the MexXY aminoglycoside efflux pump and presence of an aminoglycoside-modifying enzyme in clinical *Pseudomonas aeruginosa* isolates are highly correlated. *Antimicrob. Agents Chemother.* **65**, (2020).
60. Macvanin M., Ballagi A., Hughes D. Fusidic acid-resistant mutants of *Salmonella enterica* serovar typhimurium have low levels of heme and a reduced rate of respiration and are sensitive to oxidative stress. *Antimicrob Agents Chemother* **48**, 3877-3883 (2004).
61. Macvanin M., Johanson U., Ehrenberg M., Hughes D. Fusidic acid-resistant EF-G perturbs the accumulation of ppGpp. *Mol Microbiol* **37**, 98-107 (2000).
62. Das B., Bhadra R. K. (p)ppGpp metabolism and antimicrobial resistance in bacterial pathogens. *Front. Microbiol.* **11**, 563944 (2020).
63. Li W., *et al.* Mechanism of tetracycline resistance by ribosomal protection protein Tet(O). *Nat Commun* **4**, 1477 (2013).
64. Lang M., Carvalho A., Baharoglu Z., Mazel D. Aminoglycoside uptake, stress, and potentiation in Gram-negative bacteria: new therapies with old molecules. *Microbiol. Mol. Biol. Rev.* **87**, e0003622 (2023).
65. Rosenberg E. Y., Ma D., Nikaido H. AcrD of *Escherichia coli* is an aminoglycoside efflux pump. *J. Bacteriol.* **182**, 1754-1756 (2000).
66. Kumar A., Schweizer H. P. Bacterial resistance to antibiotics: active efflux and reduced uptake. *Adv. Drug Del. Rev.* **57**, 1486-1513 (2005).
67. Hinz A., Lee S., Jacoby K., Manoil C. Membrane proteases and aminoglycoside antibiotic resistance. *J. Bacteriol.* **193**, 4790-4797 (2011).
68. Goltermann L., Good L., Bentin T. Chaperonins fight aminoglycoside-induced protein misfolding and promote short-term tolerance in *Escherichia coli*. *J Biol Chem* **288**, 10483-10489 (2013).
69. Goltermann L., Sarusie M. V., Bentin T. Chaperonin GroEL/GroES Over-Expression Promotes Aminoglycoside Resistance and Reduces Drug Susceptibilities in *Escherichia coli* Following Exposure to Sublethal Aminoglycoside Doses. *Front Microbiol* **6**, 1572 (2015).
70. Ling J., Cho C., Guo L. T., Aerni H. R., Rinehart J., Söll D. Protein aggregation caused by aminoglycoside action is prevented by a hydrogen peroxide scavenger. *Mol. Cell* **48**, 713-722 (2012).
71. Gao Y. G., Selmer M., Dunham C. M., Weixlbaumer A., Kelley A. C., Ramakrishnan V. The structure of the ribosome with elongation factor G trapped in the posttranslocational state. *Science* **326**, 694-699 (2009).
72. Tyanova S., Temu T., Cox J. The MaxQuant computational platform for mass spectrometry-based shotgun proteomics. *Nat. Protoc.* **11**, 2301-2319 (2016).
73. Gessulat S., *et al.* Prosit: proteome-wide prediction of peptide tandem mass spectra by deep learning. *Nat. Methods* **16**, 509-518 (2019).
74. Pino L. K., Searle B. C., Bollinger J. G., Nunn B., MacLean B., MacCoss M. J. The Skyline ecosystem: Informatics for quantitative mass spectrometry proteomics. *Mass. Spectrom. Rev.* **39**, 229-244 (2020).
75. Kramer E. B., Farabaugh P. J. The frequency of translational misreading errors in *E. coli* is largely determined by tRNA competition. *RNA* **13**, 87-96 (2007).

76. Cox J., Mann M. MaxQuant enables high peptide identification rates, individualized p.p.b.-range mass accuracies and proteome-wide protein quantification. *Nat. Biotechnol.* **26**, 1367-1372 (2008).
77. Tyanova S., *et al.* The Perseus computational platform for comprehensive analysis of (prote)omics data. *Nat. Methods* **13**, 731-740 (2016).
78. Pino L. K., Searle B. C., Bollinger J. G., Nunn B., MacLean B., MacCoss M. J. The Skyline ecosystem: Informatics for quantitative mass spectrometry proteomics. *Mass Spectrom. Rev.* **39**, 229-244 (2020).
79. Mordret E., *et al.* Systematic detection of amino acid substitutions in proteomes reveals mechanistic basis of ribosome errors and selection for translation fidelity. *Mol. Cell* **75**, 427-441 e425 (2019).
80. Ducret A., Quardokus E. M., Brun Y. V. MicrobeJ, a tool for high throughput bacterial cell detection and quantitative analysis. *Nat. Microbiol.* **1**, 16077 (2016).
81. Schindelin J., *et al.* Fiji: an open-source platform for biological-image analysis. *Nat. Methods* **9**, 676-682 (2012).
82. Pettersen E. F., *et al.* UCSF ChimeraX: Structure visualization for researchers, educators, and developers. *Protein Sci.* **30**, 70-82 (2021).
83. Brown A., Long F., Nicholls R. A., Toots J., Emsley P., Murshudov G. Tools for macromolecular model building and refinement into electron cryo-microscopy reconstructions. *Acta Crystallogr. D Biol. Crystallogr.* **71**, 136-153 (2015).
84. Rohou A., Grigorieff N. CTFFIND4: Fast and accurate defocus estimation from electron micrographs. *J. Struct. Biol.* **192**, 216-221 (2015).
85. Zheng S. Q., Palovcak E., Armache J. P., Verba K. A., Cheng Y., Agard D. A. MotionCor2: anisotropic correction of beam-induced motion for improved cryo-electron microscopy. *Nat. Methods* **14**, 331-332 (2017).
86. Liebschner D., *et al.* Macromolecular structure determination using X-rays, neutrons and electrons: recent developments in Phenix. *Acta Crystallogr. D Struct. Biol.* **75**, 861-877 (2019).
87. Zivanov J., *et al.* New tools for automated high-resolution cryo-EM structure determination in RELION-3. *Elife* **7**, (2018).